# Coupled Hybrid & Electric Aircraft Design and Strategic Airline Planning

Hoogreef, M.F.M.; Zuijderwijk, N.R.; Scheers, E.; Proesmans, P.; Santos, Bruno F.

**Important note**
To cite this publication, please use the final published version (if applicable).
Please check the document version above.

# Coupled Hybrid & Electric Aircraft Design and Strategic Airline Planning

Maurice F. M. Hoogreef* , Noa Zuijderwijk[†], Elise Scheers[‡], Pieter-Jan Proesmans[§] and Bruno F. Santos[¶]
*Delft University of Technology, P.O. Box 5058, 2600GB Delft, The Netherlands*

**Electrification of aviation is regarded as one of the means to make aircraft operations less polluting and to have lower climate impact. Yet, air transportation's environmental impact depends on power train technologies and novel designs and aircraft operations within airline networks. Fully- or hybrid-electric aircraft may enter existing air transport networks through fleet replacement yet require airlines to adapt in order to operate electrified aircraft strategically. This research studies how airlines can strategically adjust their network and fleet composition when considering electrified aircraft. The novelty of this approach is to provide a direct feedback coupling between fleet planning, conceptual hybrid-electric aircraft design and climate impact minimization. Therefore, a strategic airline planning model, consisting of fleet and network analysis, is coupled to a hybrid-electric aircraft design model. A case study on the sensitivity of a regional airline network is presented to demonstrate the framework and assess the impact of trying to design aircraft and fleets with minimal climate footprint. A decrease in emissions with respect to a kerosene fleet of 11% can be achieved when a hybrid-electric fleet is designed particularly for the specified network, at the penalty of a profit decrease of 13%. Limiting fleet diversity to three types results in only 7% emissions decrease. Increasing the battery-specific energy shows an expected beneficial effect on emissions.**

## Nomenclature

**Latin Symbols**

| | | |
|---|---|---|
| $A$ | = | Aspect ratio ($\sim$) |
| $ac$ | = | Aircraft ($\sim$) |
| $b$ | = | Span ($m$) |
| $C_L$ | = | Lift coefficient ($\sim$) |
| $C_D$ | = | Drag coefficient ($\sim$) |
| $D$ | = | Drag ($N$) |
| $d$ | = | Diameter ($m$) |
| $E$ | = | Energy ($J$) |
| $e$ | = | Specific Energy ($J/kg$) |
| $e$ | = | Oswald factor ($\sim$) |
| $h$ | = | Altitude ($m$) |
| $\mathbf{K}$ | = | Set of aircraft types ($\sim$) |
| $L$ | = | Lift ($N$) |
| $l$ | = | Length ($m$) |
| $M$ | = | Mach number ($\sim$) |
| $m$ | = | Mass ($kg$) |
| $\mathbf{N}$ | = | Set of airports ($\sim$) |
| $\mathbf{P}$ | = | Set of PSO requirements ($\sim$) |
| $P$ | = | Power ($W$) |
| $R$ | = | Range ($km$) |

| | | |
|---|---|---|
| $\mathbf{R}$ | = | Set of routes ($\sim$) |
| $S$ | = | Planform area ($m^2$) |
| $t/c$ | = | Thickness-to-chord ratio ($\sim$) |
| $V$ | = | Velocity ($m/s$) |
| $W$ | = | Weight ($N$) |
| $w$ | = | Number of passengers on connected routes ($\sim$) |
| $x$ | = | Number of passengers ($\sim$) |
| $z$ | = | Flight frequency ($\sim$) |

**Greek Symbols**

| | | |
|---|---|---|
| $\eta$ | = | Efficiency ($\sim$) |
| $\Lambda$ | = | Sweep angle (deg) |
| $\lambda$ | = | Taper ratio ($\sim$) |
| $\xi$ | = | Gasturbine throttle ($\sim$) |
| $\rho$ | = | Density ($kg/m^3$) |
| $\Phi$ | = | Supplied power ratio ($\sim$) |
| $\phi$ | = | Shaft power ratio ($\sim$) |

**Superscripts**

| | | |
|---|---|---|
| $m$ | = | Route index |

---

*Assistant Professor, Faculty of Aerospace Engineering, AIAA Member, m.f.m.hoogreef@tudelft.nl
†MSc. Graduate, Faculty of Aerospace Engineering
‡MSc. Graduate, Faculty of Aerospace Engineering
§PhD Candidate, Faculty of Aerospace Engineering, AIAA Student Member
¶Associate Professor, Faculty of Aerospace Engineering

| $r$ | = | Transfer route index |
|---|---|---|

**Subscripts**

| $a$ | = | Demand origin airport index |
|---|---|---|
| $b$ | = | Demand destination airport index |
| $bat$ | = | Battery |
| $f$ | = | Fuel |
| $i$ | = | Flight start airport index |
| $j$ | = | Flight end airport index |
| $k$ | = | Aircraft type index |
| $p$ | = | Propeller |
| $s$ | = | PSO requirement between airport pair index |
| $HT$ | = | Horizontal Tail |
| $L$ | = | Landing |
| $OE$ | = | Operative Empty |
| $PL$ | = | Payload |
| $TO$ | = | Take-off |
| $VT$ | = | Vertical Tail |
| $0\_tot$ | = | Initial total (energy) |

**Abbreviations**

| AEO | = | All Engines Operating |
|---|---|---|
| AR | = | Maximum frequency of aircraft on route |

| BT | = | Block Time |
|---|---|---|
| $CO_2$ | = | Carbon di-oxide |
| DHEP | = | Distributed Hybrid Electric Propulsion |
| EI | = | Emission Index |
| FE | = | Full Electric |
| FM | = | Fuel Mass |
| HE | = | Hybrid Electric |
| IATA | = | International Air Transport Association |
| ICAO | = | International Civil Aviation Organization |
| LF | = | Load Factor |
| LTO(t) | = | Landing and Take-Off (time) |
| MDO | = | Multidisciplinary Design Optimization |
| MILP | = | Mixed-Integer Linear Programming |
| MINLP | = | Mixed-Integer, Non-Linear Programming |
| MTOM | = | Maximum Take-Off Mass |
| $NO_x$ | = | Nitrous oxides |
| OEI | = | One Engine Inoperative |
| OEM | = | Operative Empty Mass |
| PLM | = | Payload Mass |
| PREE | = | Payload Range Energy Efficiency |
| PSO | = | Public Service Obligation |
| SF | = | Stop Factor |
| TAT | = | Turnaround Time |
| TF | = | Transfer Factor |
| TLAR | = | Top-Level Aircraft Requirements |

# I. Introduction

In a bid to address and reduce the carbon footprint of aviation through design, several frameworks for hybrid-electric aircraft design and a large set of actual designs have been published over the past decade [1–13]. However, only few describe a conceptual design method that allows for the integration of hybrid-electric powertrains in the earliest aircraft design phase: the determination of the design point in a constraint diagram (or wing-thrust loading diagram) [14, 15].

Environmental impact of air transportation is not only affected by these technologies and innovative aircraft designs, but also by the way these aircraft are operated. Traditionally, the design of a new aircraft and the development of operational networks are treated independently of each other. Aircraft designers on one end, design a vehicle that satisfies the operational requirements, such as required mission range and capacity, with a certain use and flexibility in mind. Airline operators on the other hand, consider maximum vehicle characteristics and determine the best allocation of the available aircraft in the fleet. There is a potential for tighter coupling between operational planning and aircraft design, allowing for more efficient resource utilization and reduced climate impact. This can be achieved by considering fleet-and-network integrated vehicle design.

Strategic airline planning consists of fleet planning and network development[16]. Fleet planning models aim to create an optimal fleet planning for a known network (e.g., Schick and Stroup [17]). Later research also includes uncertainties [18–24] or environmental impact [25]. On the other hand, network development models aim to find the optimal network for a given aircraft fleet (e.g., Jaillet et al. [26]). Evans et al. [27] included airport capacity constraints, and Wang et al. [28] included spill and recapture of passengers.

Some attempts integrating strategic airline planning and aircraft design have been made. Crossley et al. [29] investigated the appropriate mix for both existing and yet-to-be-designed aircraft, as a "System-of-Systems" design problem (formulating the problem in a Mixed-Integer, Non-Linear Programming (MINLP) formulation). Different approaches have been presented; such as the decomposition approach of multidisciplinary optimization [29, 30] and the traditional MINLP approach for small-size problems [31]. The latter work was extended in multiple papers by incorporating uncertain passenger demand by considering the uncertainty of on-demand fractional aircraft ownership operations [32–34]. Taylor and de Weck [35, 36] showed the benefits of optimizing both the network and aircraft design at the same time and Nusawardhana and Crossley [37] and Davendralingam and Crossley [38] investigated the long-term fleet assignment and the impact on aircraft design. Different studies have been done to create an efficient algorithm and

various approaches have been presented [39–43]. Alexandre et al. [44] presented a complex integrated network approach where both the aircraft family of three aircraft designs and the air transport networks are simultaneously optimized. The integration of aircraft design so far has only considered kerosene aircraft and not the aspects of electrified aircraft. However, it is important to consider the flexibility of aircraft operations and suitability to operate from certain airfields, within a network of routes as a driver for aircraft design as demonstrated by Husemann et al. [45].

A series of successive papers is presented by Jansen and Perez on coupled optimization of aircraft design and fleet allocation using a "system-of-systems"[46, 47] approach. These cover aircraft family design and fleet assignment for minimum operating cost and fuel burn for a fixed deterministic trip demand in [48], uncertain passenger demand [49], passenger preferences [50] and including route networks in North America and Europe and comparing the trade-offs between different markets [51]. Additionally, instead independently optimizing a single aircraft for single markets, Jansen and Perez [52] present the coupled optimization of a family of aircraft with network allocation while considering operations in multiple markets. In 2021, Reid et al. [53] use this framework to assess impact of carbon pricing on a regional network though without redesigning the aircraft. The trade-off between cost en climate impact has been previously assessed by Schwartz and Kroo [54]. Bower and Kroo [55] performed a multi-objective aircraft optimization of a single-aisle conceptual aircraft considering the economic and environmental performance, to minimize the operating cost, $CO_2$ emissions and $NO_x$ emissions of a fleet over the route network. Govindaraju et al. [56] also performed a multi-objective optimization for concurrent aircraft design and fleet assignment and examined the trade-offs between the reduction of fleet-level fuel consumption and some defined fleet-level performance metrics.

An article by Weit et al. [57] considers the network-optimized design of a hybrid-electric aircraft, where the hybridization ratio is varied to maximize aircraft direct operating profit. This couples a network model, a vehicle model, and an economics model. The network model considers the routes within the network of Cape Air. The vehicle model uses a Pilatus PC-12 as a baseline, with its propulsion system modified to a hybrid-electric architecture. Outer shape, empty weight and maximum take-off weight of the original aircraft are fixed, and as such, the power requirements for each phase of the mission are directly obtained from the PC-12 aircraft. Economic profit is calculated through a parametric cost build-up as described by Roskam [58], modified to account for hybrid-electric propulsion systems.

So far, no integrated strategic airline planning and aircraft design for (hybrid-) electric aircraft has been presented in the literature which also includes airport characteristics (runway length) and climate impact while designing a fleet of network to best fit a market. This is trickier for hybrid-electric aircraft due to the unknown presence of charging facilities. This article presents such a strategic airline planning model for hybrid-electric aircraft, as developed in the CHYLA project[a], coupled and integrated with hybrid-electric aircraft design for climate optimized aircraft. The aim is to integrate aircraft fleet and network analysis with aircraft design to design a fleet for a regional airline network with reduced climate impact, while considering operational constraints. The present work relies on an aircraft design framework developed by Proesmans and Vos [59], extended with methods from de Vries et al. [14] and Finger et al. [15]. The former framework has been developed for the GLOWOPT project[b].

We follow a two-stage approach to achieve this objective. First, we study a regional airline network operating on a database of hybrid-electric and kerosene aircraft, which can be scaled linearly around their design point (trading energy storage capacity and payload mass). This is considered in case study 1. The second stage (case study 2) uses a coupled climate optimized aircraft design/strategic airline planning by adapting the MDO framework mentioned earlier [59]. This coupling allows for larger variations in the aircraft design.

Currently realized battery-specific energy for a demonstrator aircraft reached 207 Wh/kg at cell level for the Airbus E-Fan.[c] Densities of up to 400-600 Wh/kg at pack level by 2035 have been predicted [8, 60, 61]. However, typical conceptual aircraft designs often require a specific energy of 500-750 Wh/kg [3, 62–64]. As increasing the specific energy is already challenging, it is more likely for hybrid-electric aircraft to become feasible in the future than fully-electric aircraft. Hence, application of such aircraft is likely restricted to commuter and perhaps regional aircraft.[d]

We propose the coupling approach in more detail in Section II. Section II.B and Section II.C describe the aircraft design model and the strategic airline planning model, respectively. Validation of both models is presented in Section III before presenting the case studies on a regional airline network. Following the earlier description, this will be presented in two case studies in Section IV and Section V. Conclusions are presented in Section VI.

---

[a]EU Horizon 2020 thematic topic: Credible HYbrid eLectric Aircraft - CHYLA https://cordis.europa.eu/project/id/101007715

[b]EU Horizon 2020 thematic topic: Global-Warming-Optimized Aircraft Design - GLOWOPT https://cordis.europa.eu/project/id/865300

[c]ICAO 2016 Environmental Report - On Board a Sustainable Future https://www.icao.int/environmental-protection/Documents/ICAO%20Environmental%20Report%202016.pdf

[d]ATAG Waypoint 2050 - https://aviationbenefits.org/environmental-efficiency/climate-action/waypoint-2050/

## II. Methodology

Figure 1 illustrates the overall model coupling proposed in this paper. A set of aircraft designs feeds an initial aircraft database from which the fleet and network model can select the aircraft to use in a particular input network. The network performance is evaluated in terms of an objective, for example minimum climate impact or cost. The off-design performance analysis may propose the use of larger or smaller aircraft or suggest different design ranges as these could be more optimal in the chosen network. A feedback loop is constructed to the aircraft design framework to perform aircraft redesigns and update the database accordingly. This section describes coupling strategy (Section II.A), the aircraft design model in Section II.B, the strategic airline planning, composed of the fleet and network model, in Section II.C, climate optimization Section II.D and off-design aircraft performance estimation Section II.E.

### A. Coupling Strategy

The design of a hybrid-electric aircraft fleet for a particular airline network which contributes to a lower climate impact, is achieved by integrating: hybrid-electric aircraft design , fleet-and-network allocation , and climate optimization. These are executed sequentially and multiple iterations on aircraft design and strategic airline planning are performed to identify the fleet best suited to the given network. Toplevel aircraft inputs and performance indicators are shown between curly brackets in Figure 1, performance indicators of the network will be compared in each iteration to determine whether new aircraft designs are required.
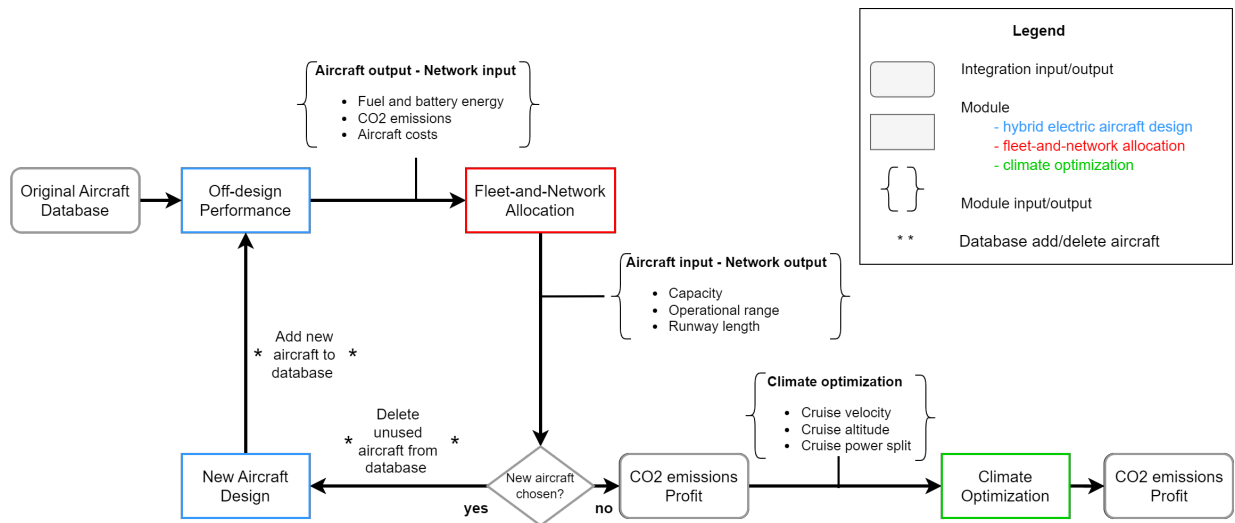


**Fig. 1   Coupling strategy workflow**

The process illustrated in Figure 1 first requires a set of input aircraft, referred to as the original aircraft fleet. These aircraft and their respective performance indicators, are stored in an aircraft database. Adaptations will be made to the design inputs of these aircraft. The network performance is directly related to the aircraft operating in the airline network. The aircraft operations are largely defined by the number of passengers an aircraft can carry over a route distance between two or more airports and the possible airports the aircraft can operate at. The latter is currently limited by the minimum runway length. It is therefore interesting to find the best combinations of capacity-range-runway to optimally serve the network according to network-level objectives, such as profit or total emissions. In each design iteration, changes will be made to the existing aircraft in terms of required aircraft capacity, maximum operating range, and required runway length. The strategy to achieve this is threefold consisting of (1) an off-design performance investigation, (2) a fleet-and-network allocation and (3) new aircraft design propositions.

### B. Aircraft Design

Hybrid-electric aircraft are designed for a set of top-level aircraft requirements (TLARs). To directly couple the Aircraft Design module with the Fleet-and-Network Allocation module, it is required to be robust and computationally inexpensive. Nonetheless, it should be able to capture the discipline interactions and trade-offs of hybrid-electric aircraft design. This is achieved by developing a conceptual aircraft design tool based on analytical and semi-empirical

methods. An existing aircraft design tool developed by Proesmans and Vos [59] is adapted and extended to implement hybrid-electric propeller aircraft, using the methodology presented by de Vries [65]. The Extended Design Structure Matrix (XDSM) in Figure 2 shows the iterative hybrid-electric aircraft design set-up. The aircraft design module is governed by the Initializer and the Synthesizer/Converger.
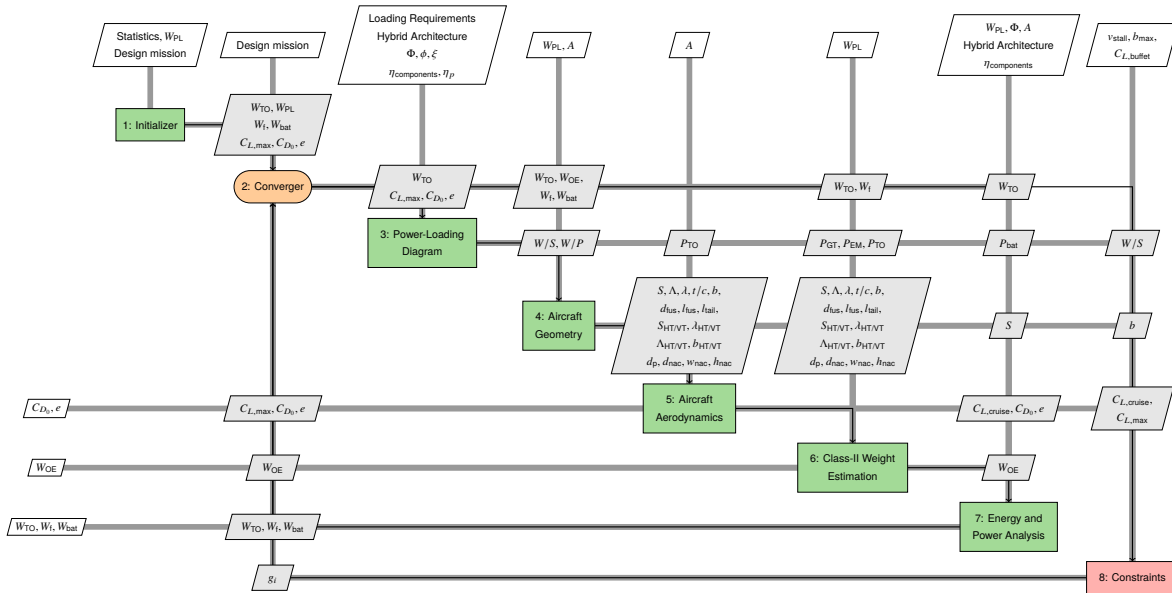


**Fig. 2   XDSM of Hybrid-Electric aircraft design module**

This paper primarily focuses on aircraft with a parallel hybrid-electric powertrains. The hybrid powertrain is represented through a simplified model including energy sources, nodes, components which transform one type of power into another and the power paths which connect these elements. Batteries and electrical machines with rectifiers and converters are not modelled specifically as they do not change the type of power transmitted. They are solely characterized by a transmission efficiency, gravimetric and volumetric energy and power. Other components such as cables, cooling and switches are combined in a power-management and distribution element. A notional drawing is presented in Figure 3. Here F is the fuel, GT is the gas turbine, GB is the gearbox, P1 is the propeller, EM is the electric motor, BAT is the battery, and PMAD is the power-management and distribution.
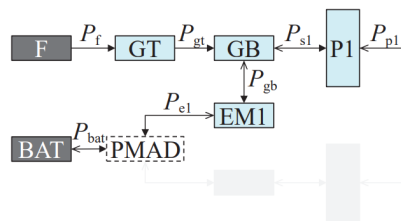


**Fig. 3   Parallel hybrid powertrain architecture from de Vries [65]**

### 1. Initializer
The Initializer is run once and uses the design mission profile and required payload mass to design a reference kerosene aircraft using a Class-I weight estimation method with fuel fractions and statistical aerodynamics data from Roskam [58]. In the next step, the aircraft is updated to a hybrid-electric configuration.

### 2. Hybrid-Electric Aircraft Design
The aircraft synthesizer iterates over five disciplines and updates the initial input values until convergence of the design in terms of maximum take-off mass (MTOM) and operating empty mass (OEM). The hybrid-electric design disciplines

are shown in green in Figure 2 and consist of:
1) Power-loading Diagram
2) Aircraft Geometry
3) Aircraft Aerodynamics
4) Class-II Weight Estimation
5) Energy and Power Analysis

### 3. Power-Loading Diagram

The power-loading diagram shows the power-loading ($W/P$) ratio versus the wing loading ($W/S$) and constrains the feasible design space. An example is shown in Figure 4 for requirements on stall speed, take-off length, cruise speed, and climb gradient in one-engine-inoperative (OEI) condition. The green colored area shows the feasible design space, the red diamond shows the design point at the maximum feasible $W/S$ and highest feasible $W/P$. This selected design point typically minimizes the maximum take-off mass of the aircraft.
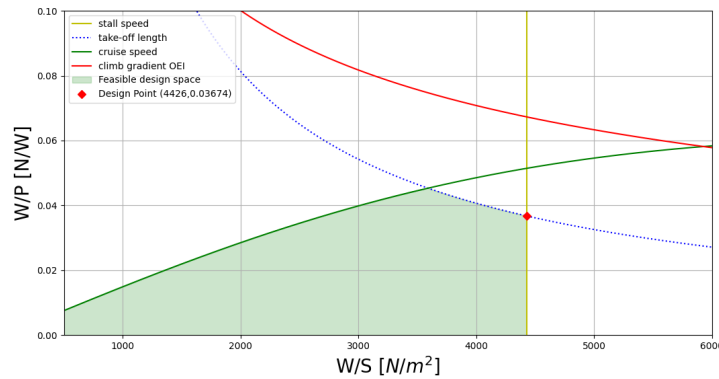


**Fig. 4    Example aircraft power-loading diagram**

For hybrid-electric aircraft, the power-loading diagram can be split into multiple diagrams for each component in the powertrain defined in Figure 3. The powertrain matrix described by de Vries et al. [66] is used to deduce the power requirements of the different powertrain components. This approach uses (constant) powertrain component efficiencies ($\eta$) and aircraft propulsive power ($P_p$) as an input. The propulsive power is obtained from the power-loading values of each constraint in the aircraft level power-loading diagram. Additionally, the designer is required to specify three power control parameters for each constraint:

- The supplied power split ratio, which represents the ratio of amount of power drawn from the electrical energy source with respect to the total amount of power drawn from all energy sources (Equation 1). For parallel hybrid-electric aircraft, this value is between 0 and 1, in case the battery is being discharged.
- The shaft power ratio, which represents the ratio of shaft power produced by secondary electrical machines with respect to the total shaft power (Equation 2). For parallel architectures, this value is always equal to 0.
- The gas-turbine throttle, which represents the power produced by the gas turbine with respect to the maximum power it can produce and takes a value between 0 and 1 for parallel hybrid-electric architectures (Equation 3).

$$\Phi = \frac{P_{bat}}{P_{bat} + P_f} \qquad (1) \qquad \phi = \frac{P_{s2}}{P_{s2} + P_{s1}} \qquad (2) \qquad \xi_{GT} = \frac{P_{GT}}{P_{GT_{max}}} \qquad (3)$$

### 4. Aircraft Geometry

The conceptual aircraft geometry is generated for fuselage, main wing, horizontal tail, vertical tail and propeller. The sizing equations are obtained from the conventional aircraft sizing methods presented by Torenbeek [67]. The turboprop dimensions, including the propeller diameter, length, height, and width of the nacelle are obtained from Thijssen [68]. The initial sizing of the hybrid-electric aircraft does not differ from the conventional methods; however volume constraints are considered for the battery. The battery is located in the wing together with the fuel in order to keep the additional mass as close as possible to the center of gravity and thus limit the effects on aircraft stability. If the wing volume does not suffice, the battery will be located in the fuselage compartment under the floor.

### 5. Aircraft Aerodynamics

The aircraft geometry for aerodynamic analysis is divided into different components: wing, fuselage, nacelles, and empennage. The drag coefficient ($C_D$, $C_{D_0}$) and Oswald efficiency factor ($e$) are updated according to the method from Obert [69]. The profile drag of all components is determined and related to the flat plate skin friction coefficient using shape factors. Effect of landing gear and flap settings on the clean zero-lift drag coefficient and oswald efficiency factor are included in the factors $\Delta C_{D_0}$ and $\Delta e$ according to the corrections outlined by Roskam [58].

### 6. Class-II Weight Estimation

A component weight estimation is used to determine the operational empty weight according to the methods by Torenbeek [67]. The hybrid-electric powertrain weight is estimated from the (equivalent) specific power values of the gas turbine and electric motor and their respective required powers obtained from the component-level power-loading diagrams. The specific power value for the electric motor is a design input and can be obtained from state-of-the art literature. A total weight penalty of 30% is included in the equivalent specific power for the electric motor to account for cooling, converters and cables for thermal and power management systems. The specific power of the gas turbine is calculated using the relations by Teeuwen [70], propeller mass is added separately from correlations presented by Teeuwen [70].

### 7. Energy and Power Analysis

A mission analysis to determine required energy and power is performed, estimating fuel and battery mass. A design mission profile including reserve fuel requirements is sketched in Figure 5. The design mission comprises of:
- A harmonic mission, where the cruise range is defined at maximum passenger capacity.
- A diversion mission of 100 NM range at an altitude of 5000 ft.
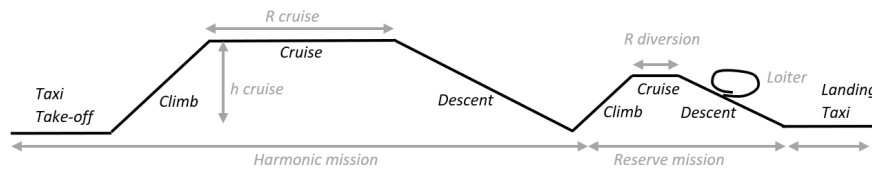- An endurance mission of 45 minutes at 1500 ft altitude.



**Fig. 5    Design mission profile**

A simplification with respect to the time-stepping approach by de Vries et al. [66] is used, instead using the hybrid range equation derived by de Vries et al. [71] is used to calculate the required energy during the cruise phase of the mission. The energy required during the other mission phases is obtained using fuel and energy fractions, combustion and electrical efficiencies and a constant power split value. The battery state-of-charge is limited to twenty percent and the critical condition for battery sizing is determined from both energy and power requirements.

### 8. Synthesizer/ Converger and Constraints

The synthesizer checks convergence of the aircraft design within a specified tolerance level. Additionally, constraints are added to the design space to make a realistic aircraft design. These constraints are verified manually after the convergence. The following three constraints are included:
- The determined wing loading is smaller or equal than the one for stall speed: $W/S \leq W/S_{\text{stall}}$;
- The lift coefficient during cruise is lower than the buffet onset value: $C_{L_{\text{cruise}}} < C_{L_{\text{buffet}}}$ ;
- The wingspan is limited to the maximum wing span of ICAO type C gates at 36 meters: $b \leq 36m$.

## C. Strategic Airline Planning

The network and fleet model is based on Reference [22] and is adapted to consider operation of electrified aircraft. The input of the model is presented in Section II.C.1 and its objective is to maximize profit. This can be achieved by assigning passengers to flights and assigning flights to aircraft. The model can consider direct and connecting passengers,

transferring between flights at specific airports. The results provide network performance in terms of revenue, cost, $CO_2$ emissions, network configuration, flight frequencies, and passenger flows, and fleet diversity and allocation.

Compared to the operation of kerosene aircraft, electrified aircraft need to be recharged. For this particular application it is assumed that the recharging of aircraft is done by a battery swap method, though this mainly affects turnaround time and airport facilities. Not every airport has a charging or swapping facility, and therefore, the network should be defined in routes instead of single flights. One route consists of one or multiple subsequent flights and starts and ends at an airport with a charging facility. Intermediate stops do not need a charging facility. Furthermore, the routes with a total distance longer than the maximum aircraft range and routes with airports with a smaller runway than the required minimum aircraft runway are not considered.

### 1. Model Input

The required input consists of network information and an initial aircraft database. Airports, with an ICAO or IATA code and a maximum runway size, define the network. Furthermore, the availability of refueling and recharging facilities should be provided per airport. The distance between and passenger demand for each airport pair should also be given. Other required information includes the maximum time aircraft can be operated per day, which is referred to as the *maximum daily block time*.

The model input also requires the definition of the duration of the planning that must be made, which could be one day, a week, or even multiple years. As it is unlikely that all future flights will be completely filled, a *load factor* is used to capture the expected average aircraft seat occupation in the future. Some regional airlines operate in low-demand markets in which the government may define minimum capacity and frequency per route according to public service obligations or PSOs. These are guaranteed in exchange for pre-defined compensation. Our model can consider these PSOs requirements and compensations.

Revenue can be defined by passenger-kilometer for the entire network or per airport pair. In the network, passengers can have an extra stop between their origin and destination. The yield for having an extra stop can be multiplied by a *stop factor*, which is a value between 0 and 1 to penalize extra required stops. Furthermore, passengers may transfer to different flights, for which an additional *transfer factor* between 0 and 1 is included in the yield calculation.

A database of available aircraft for use in the network should be provided, from which a fleet is selected. These aircraft require the following inputs: number of seats, speed, required runway distances, and maximum range, as well as information on battery and fuel capacity, battery energy and fuel consumption per kilometer, and battery energy and fuel consumption per landing and take-off cycle. Furthermore, time estimations for turnaround without reloading (thus refueling and recharging), reloading, and the landing and take-off cycles must be provided. In this study, the reloading is considering as the refueling or recharging of the aircraft. The boarding of passengers and cargo (un)loading is included in the turnaround time without reloading.

The ownership cost per aircraft and operating cost per flight are considered. The ownership cost is defined per aircraft per day. The operating cost is determined per aircraft per flight leg and consists of a fixed cost, time-based cost, distance-based cost, fuel cost, and battery energy cost. Fixed cost represents airport use, landing rights, and parking fees, and depends on the aircraft type and the number of flights. Furthermore, time-based costs are defined per block hour and account for the cabin and flight crew. Distance-based costs depend on the flown kilometers and represent costs such as maintenance. $CO_2$ tax and fuel and energy costs are added to the operating cost. Hence, values for the $CO_2$ emission per kg kerosene, the $CO_2$ tax in €/kg, fuel cost and energy cost should be provided.

### 2. Network and Fleet Model

This section defines the formulation of the network and fleet model. This formulation consists of sets, parameters, performance calculations, decision variables, the objective function, and constraints. Based on existing network and fleet models [22] and the additional model elements, a Mixed Integer Linear Programming (MILP) model is built to optimize the network to the objective function. This MLIP problem is solved through Gurobi [72].

**Sets, Parameters, and Performance Calculations**

The following **sets** are present in the model formulation. Note that a *flight* is used for a single flight leg and a *route* for a set of flight legs conducted by the same aircraft, right after each other.

- *N*: set of airports, indexed by:
    - *i* : used for flight start airport
    - *j* : used for flight end airport

  – $a$: used for demand origin airport
  – $b$: used for demand destination airport
- $R$: set of routes, indexed by:
  – $r$: used for route
  – $m$: used for transfer route
- $K$: set of aircraft types, indexed by $k$
- $P$: set of PSO requirements for direct flights per airport pair, indexed by $s$

To interpret the formulation, the following abbreviations and explanations of parameters are provided:
- $LF$ : load factor
- $BT$ : maximum daily block time
- $TAT$ : turnaround time
- $LTOt$ : landing and take-off time
- $SF$ : stop factor
- $TF$ : transfer factor
- $period$ : time span in days
- $PSOcap_s$ : minimum PSO capacity on flight $s$
- $PSOfreq_s$ : minimum PSO frequency on flight $s$

Passengers in this model are allocated to routes instead of single flights. To do this, additional parameters are set to connect demand and flights to routes. These binary parameters are:
- $R1^r_{i,j}$, this equals 1 if flight $i$ to $j$ is part of route $r$
- $R2^r_{a,b}$, this equals 1 if route $r$ can transport passengers from $a$ to $b$
- $R3^r_{a,b_{i,j}}$, this equals 1 if on route $r$, travelling from $a$ to $b$, flight $i$ to $j$ is taken
- $R4^{r,m}_{a,b}$, this equals 1 if route $r$ followed by route $m$ can transport passengers from $a$ to $b$
- $stops^r_{a,b}$, $stops^{r,m}_{a,b}$, the number of extra stops on route $r$ (and $m$) for a passenger travelling from $a$ to $b$
- $SR^r_s$, this equals 1 if route $r$ is contributing to the PSO requirement $s$

As the model assigns routes to aircraft, the performance of each aircraft per route needs to be determined. First of all, the required fuel and battery energy per route per aircraft type are determined in Equations (4) and (5). In these equations, the $flights_r$ parameters indicates the number of flights on route $r$. If the required fuel and battery energy can be stored in the aircraft and the runway size complies, the route can be flown by the aircraft type and parameter $AR$ is adjusted, see Equation (6). If the aircraft type can fly the route, the other performance values, such as emission, time, and cost, are determined as presented in equation Equations (7) to (9). Note that we assume that at the start of each route, the aircraft is reloaded (thus recharged and/or refueled). Therefore, the cost definition shows the operating cost. The total emissions are calculated as the sum of the aircraft emissions of a certain aircraft type on a route ($emission^r_k$, see Section II.C.3) times the frequency of that aircraft on the route ($z^r_k$), for a given period of time.

$$fuel^r_k = fuel\_per\_km_k * distance_r + fuel\_per\_LTO_k * flights_r \tag{4}$$

$$battery^r_k = battery\_per\_km_k * distance_r + battery\_per\_LTO_k * flights_r \tag{5}$$

$$AR^r_k = 10000 \quad \text{if route } r \text{ can be flown by aircraft } k, \text{ else value is } 0 \tag{6}$$

$$emission^r_k = emission\_fuel * fuel^r_k \tag{7}$$

$$time^r_k = distance_r / speed_k + (LTOt + TAT) * flights_r + reload\_time_k \tag{8}$$

$$cost^r_k = cost\_trip_k * flights_r + cost\_hour_k * time^r_k + cost\_km_k * distance_r \tag{9}$$
$$+ fuel\_cost * fuel^r_k + energy\_cost * batt^r_k + CO_2\_tax * emission^r_k$$

**Decision Variables**
The following four decision variables are used to control the allocation:
- $ac_k$ : Amount of aircraft needed from type $k$
- $z^r_k$ : Frequency of aircraft $k$ on route $r$ in given period
- $x^r_{a,b}$ : Number of passengers that go from airport $a$ to $b$ on route $r$ in given period
- $w^{r,m}_{a,b}$ : Number of passengers that go from airport $a$ to $b$ on route $r$ followed by route $m$ in given period

**Objective Function**

The objective function (OF) can be defined based on the objective of the airline. Generally, the objective of an airline is to maximize profit, thus maximizing the revenue minus cost (see Equation (10)). The formulation for revenue is given in Equation (11) and for cost in Equation (12).

$$\textit{maximize } \text{OF} = \textit{maximize } \text{Profit} = \textit{maximize } (\text{Revenue} - \text{Cost}) \tag{10}$$

$$
\begin{aligned}
\text{Revenue} = \sum_{r \in \boldsymbol{R}} \sum_{a \in \boldsymbol{N}} \sum_{b \in \boldsymbol{N}} \Big[ & yield_{a,b} * dist_{a,b} * SF^{stops^r_{a,b}} * x^r_{a,b} \\
& + \sum_m [yield_{a,b} * dist_{a,b} * TF * SF^{stops^{r,m}_{a,b}} * w^{r,m}_{a,b}] \Big]
\end{aligned}
\tag{11}
$$

$$\text{Cost} = \sum_{k \in \boldsymbol{K}} \Big[ \sum_{r \in \boldsymbol{R}} [cost^r_k * z^r_k] + cost\_ownership_k * ac_k \Big] \tag{12}$$

**Set of Constraints**

The constraints include the following sets of inequalities: Equation (13) ensures that the total sum of passengers that travel from airport $a$ to $b$ should be smaller or equal to the demand from airport $a$ to $b$.

$$\sum_{r \in \boldsymbol{R}} \left[ x^r_{a,b} + \sum_m w^{r,m}_{a,b} \right] \leq demand_{a,b} \qquad \forall a, b \in \boldsymbol{N} \tag{13}$$

Set of constraints Equation (14): number of passengers that travel from $a$ to $b$ on route $r$ is less or equal to the demand from $a$ to $b$ if route $r$ can serve demand from $a$ to $b$.

$$x^r_{a,b} \leq demand_{a,b} * R2^r_{a,b} \qquad \forall a, b \in \boldsymbol{N}, r \in \boldsymbol{R} \tag{14}$$

Set of constraints Equation (15): number of passengers that travel from $a$ to $b$ on route $r$ followed by route $m$ is less or equal to the demand from $a$ to $b$ if route $r$ and $m$ combined can serve demand from $a$ to $b$.

$$w^{r,m}_{a,b} \leq demand_{a,b} * R4^{r,m}_{a,b} \qquad \forall a, b \in \boldsymbol{N}, r, m \in \boldsymbol{R} \tag{15}$$

Set of constraints Equation (16): the flow of passengers from airport $i$ to $j$ on route $r$ should be less or equal to the total seats on aircraft flying from airport $i$ to $j$ on route $r$.

$$
\begin{aligned}
\sum_{a \in \boldsymbol{N}} \sum_{b \in \boldsymbol{N}} \Bigg[ x^r_{a,b} * R3^r_{a,b_{i,j}} + \sum_m \Big[ w^{r,m}_{a,b} * R3^r_{a,end_{r_{i,j}}} * R4^{r,m}_{a,b} \Big] + \sum_m \Big[ w^{m,r}_{a,b} * R3^r_{start_r,b_{i,j}} * R4^{m,r}_{a,b} \Big] \Bigg] \\
\leq \sum_k \Big[ R1^r_{i,j} * z^r_k * seats_k * LF \Big] \qquad \forall r \in \boldsymbol{R}, i, j \in \boldsymbol{N}
\end{aligned}
\tag{16}
$$

Set of constraints Equation (17): aircraft can only fly route $r$ with aircraft type $k$ if possible.

$$z^r_k \leq AR^r_k \qquad \forall k \in \boldsymbol{K}, r \in \boldsymbol{R} \tag{17}$$

Set of constraints Equation (18): for all start and end (charging airports), the number of aircraft landings should be equal to the number of aircraft take-offs.

$$\sum_r \left[ \sum_{i \in \boldsymbol{N}} \Big[ R1^r_{i,c} \Big] * z^r_k \right] = \sum_m \left[ \sum_{j \in \boldsymbol{N}} \Big[ R1^r_{c,j} \Big] * z^m_k \right] \qquad \forall k \in \boldsymbol{K}, c \in \boldsymbol{N}_{charging=possible} \tag{18}$$

Set of constraints Equation (19): maximum time an aircraft is used should be smaller or equal to the total block time.

$$\sum_{r \in \boldsymbol{R}} \Big[ time^r_k * z^r_k \Big] \leq BT * ac_k * period \qquad \forall k \in \boldsymbol{K} \tag{19}$$

10

Set of constraints Equation (20) and Equation (21): fulfill PSO requirements, for frequency requirements and for capacity requirements, respectively.

$$\sum_{r \in \mathbf{R}} \left[ SR_s^r * \sum_{k \in \mathbf{K}} z_k^r \right] \geq PSO freq_s \qquad \forall s \in \mathbf{P} \tag{20}$$

$$\sum_{r \in \mathbf{R}} \left[ SR_s^r * \sum_{k \in \mathbf{K}} \left[ seats_k * z_k^r \right] \right] \geq PSOcap_s \qquad \forall s \in \mathbf{P} \tag{21}$$

*3. Aircraft Performance*

Each aircraft in the airline fleet is characterized by the following design parameters: aircraft capacity, maximum mission range, required runway length, operating cruise speed, operating cruise altitude and operating cruise power split. The performance of each aircraft is measured by the performance indicators: fuel and battery energy capacity, $CO_2$ emissions, operating times and aircraft cost.

**Fuel and Battery Energy Capacity**

An aircraft is designed for a harmonic mission, consisting of a climb-and-descent cycle and a cruise phase. The climb-and-descent cycle consists of the taxi, takeoff, climb, descent, and landing phase. The cruise phase is executed over a given range value ($R\_cruise$). Each aircraft is characterized by the following parameters:

- The amount of fuel and battery energy required for a climb-and-descent cycle:
  $fuel\_climb\_descent_k$ and $energy\_climb\_descent_k$;
- The amount of fuel and battery energy required per flown kilometer in cruise:
  $fuel\_km_k$ and $energy\_km_k$;
- The maximum amount of fuel and battery energy required to fly the harmonic mission:
  $max\_fuel_k$ and $max\_energy_k$.

Calculating the maximum fuel and battery energy is straightforward en given by Equations (22) and (23).

$$max\_fuel_k = fuel\_km_k \cdot R\_cruise_k + fuel\_climb\_descent_k \tag{22}$$

$$max\_energy_k = energy\_km_k \cdot R\_cruise_k + energy\_climb\_descent_k \tag{23}$$

An aircraft operating between an origin airport $a$ and destination airport $b$ can do this either by a direct flight, or by having an additional stop at another airport $c$. The two corresponding route profiles are visualized in Figures 6 and 7. To calculate the amount of fuel and battery energy required to fly a certain mission, Equations (24) and (25) are used, where $R\_cruise\_route^r$ is the cruise distance flown for the route and $route\_stops^r$ are the stops on that route.
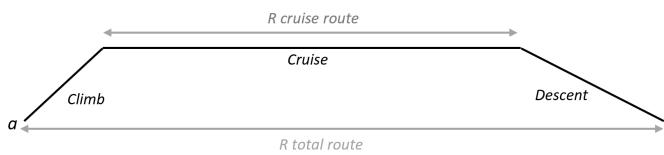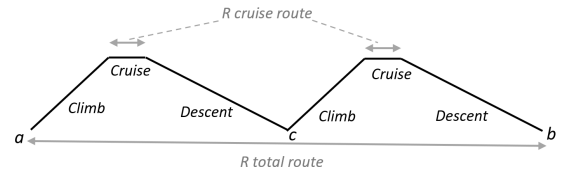


**Fig. 6   Route profile for a 1-stop mission**



**Fig. 7   Route profile for a 2-stop mission**

$$fuel_k^r = fuel\_km_k \cdot R\_cruise\_route^r + fuel\_climb\_descent_k \cdot route\_stops^r \tag{24}$$

$$energy_k^r = energy\_km_k \cdot R\_cruise\_route^r + energy\_climb\_descent_k \cdot route\_stops^r \tag{25}$$

To determine whether a certain aircraft type can fly a given route, the fuel and battery energy required to fly the route should be lower or equal to the maximum defined by the aircraft **and** the runway length required by the aircraft to take-off and land should be smaller or equal to the minimal runway length on the route. The resulting statements are listed in Equation 26. If all the inequalities in Equation (26) hold, the parameter $AR_k^r$ is set to 10000, according to Equation (6).

$$fuel_k^r \leq max\_fuel_k \quad \text{and} \quad energy_k^r \leq max\_energy_k \quad \text{and} \quad min\_runway^r \geq runway_k \tag{26}$$

11

**CO$_2$ Emissions**

Equations (24) and (25) indicate the amount of fuel and battery energy required to fly a certain route $r$ with aircraft type $k$. From this, it is possible to estimate the CO$_2$ emissions of this aircraft on the particular route as the CO$_2$ emissions are directly related to the amount of fuel and battery energy required through emission indices. The emission indices used are those shown in Table 1 for in-flight fuel burn, on-ground kerosene production and on-ground electricity production. The emission calculation is given in Equation 27.

$$
\begin{aligned}
emissions_k^r = \quad & EI\_kerosene\_inflight \cdot fuel_k^r \; + \\
& EI\_kerosene\_onground \cdot fuel_k^r \; + \\
& EI\_electricity\_onground \cdot energy_k^r
\end{aligned}
\tag{27}
$$

**Table 1    CO$_2$ emission indices for several operations [73]**

| EI kerosene inflight | EI kerosene onground | EI electricity onground |
|---|---|---|
| 3.155kg CO$_2$/ kg fuel | 478.22g CO$_2$/kg fuel | 30.01g CO$_2$/ kWh electricity |

**D. Climate Optimization Module**

The climate optimization module is responsible for optimizing hybrid-electric aircraft for minimal climate impact. The effects of the operational cruise velocity, cruise altitude, and cruise power split are investigated through a design space exploration study. Climate impact is measured by the amount of total CO$_2$ emissions. Thijssen [68] shows that for low altitude operations of propeller aircraft, the climate impact is governed by the CO$_2$ emissions and short-lived emissions dependent on fuel burn. The total CO$_2$ emissions are the sum of the CO$_2$ emissions coming from burning fuel in-flight, the production of kerosene on-ground, and the electricity production on-ground. In addition to kerosene and electricity production, also battery production causes CO$_2$ emissions. This contribution was neglected as life cycle assessment studies show dominance of the operational phase [73]. Furthermore, there is a large uncertainty in assessing life-cycle emissions for battery production due to the variety of methods and materials used in manufacturing. The order of magnitude can vary from 56 to 494 kg CO$_2$/$kWh$.[e] Emission indices for fuel burn, fuel production and electricity production are shown in Table 1. Electricity production assumes renewable energy sources.

**E. Off-design Performance**

In this study, aircraft are designed for a harmonic range defined at maximum structural payload. This point is hereafter referred to as the 'on-design' aircraft. In typical networks, aircraft operate at payload-range combinations different from this design point. In the off-design performance investigations, trade-offs are made for existing aircraft without changing the design itself. These trade-offs are captured by a payload-range trade-off and a payload-runway trade-off.

*1. Payload vs. Range*

For conventional kerosene aircraft, it is possible to decrease the payload mass in order to take more fuel and such increase the aircraft range. However, when decreasing the payload mass, the frequency of certain routes might need to increase in order to meet the desired passenger demand, which in terms increases the cost of operating the aircraft. This payload-range trade-off can be captured by the well-known Breguet range equation.

However, for hybrid-electric aircraft, battery mass plays an important role. In this case, the range equation can better be expressed as a trade-off between payload mass and aircraft energy. de Vries et al. [71] derived this equation for hybrid-electric aircraft with constant power split, as shown in Equation 28.

$$
R = \eta_3 * \frac{e_f}{g} * \frac{L}{D} * \left( \eta_1 + \eta_2 * \frac{\phi}{1 - \phi} \right) * \ln \left( \frac{W_{OE} + W_{PL} + W_f + W_{bat}}{W_{OE} + W_{PL} + W_{bat}} \right)
\tag{28}
$$

---

[e]Effects of battery manufacturing on electric vehicle life-cycle greenhouse gas emissions, International Council on Clean Transportation, 2018 https://theicct.org/sites/default/files/publications/EV-life-cycle-GHG_ICCT-Briefing_09022018_vF.pdf

Here, $R$ is the maximum range ($m$), $\eta_1, \eta_2$ en $\eta_3$ are conversion or transmission efficiencies ($-$), $e_f$ and $e_b$ the specific fuel and battery energy ($J/kg$), $g$ the gravitational acceleration ($m/s^2$), $L/D$ the lift over drag ratio in cruise ($\sim$), $W_{OE}$ the operating empty weight of the aircraft without batteries ($N$), $W_{PL}$ the payload weight ($N$), $W_f$ the fuel weight ($N$), $W_b$ the battery weight ($N$), $\phi$ the supplied power ratio of the battery ($\sim$), and $E_{0\_tot}$ the total energy at the start ($GJ$). The equation is valid if the supplied power split, flight speed, lift-to-drag ratio and transmission efficiencies are constraint throughout the cruise phase.

It must be noted that during the payload-range trade-off, the battery mass is kept constant at the harmonic design point. However, some additional energy is required at larger ranges which was originally provided by the extra battery mass. This additional energy will therefore be provided by some extra fuel as shown in Equations (29) to (32), where $m_{bat}$ is the battery mass from the original payload-range trade-off, $m_{bat_{harm}}$ is the battery mass at the harmonic design point and $m_{bat_{upd}}$ is the final battery mass. Similarly, $m_f$ is the fuel mass from the payload-range trade-off and $m_{f_{upd}}$ is the final fuel mass.

$$\Delta m_{bat} = m_{bat} - m_{bat_{harm}} \quad (29)$$

$$m_{bat_{upd}} = m_{bat_{harm}} \quad (31)$$

$$\Delta m_f = \frac{e_b}{e_f} \cdot \Delta m_{bat} \quad (30)$$

$$m_{f_{upd}} = m_f + \Delta m_f \quad (32)$$

As a consequence, the take-off mass is slightly decreasing due to the fact that the additional battery energy required is now delivered by additional fuel which has a much larger specific energy, and therefore less weight. One could also opt to again add more payload and/or more fuel in order to keep the take-off weight constant. This was however not implemented as it was decided that the energy required to fly the mission should not change, significantly simplifying the analysis. The decrease in take-off weight will in term cause the aircraft to be able to take off and land from shorter runways. Furthermore, due to the extra fuel and constant battery mass, the power split value is not constant but slightly decreasing with increased range. This results in a new payload-range trade-off as seen in Figures 8 and 9.
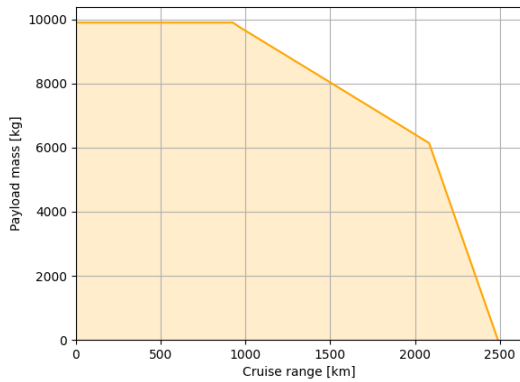


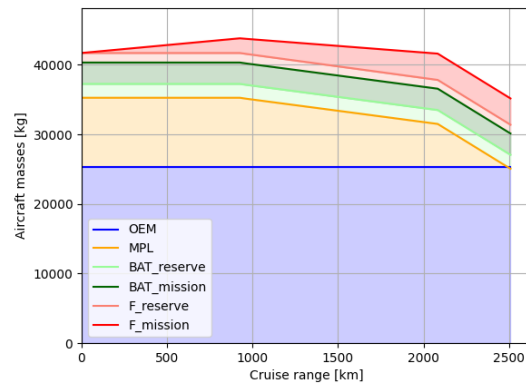Fig. 8    Payload-range (constant battery mass)



Fig. 9    Aircraft masses (constant battery mass)

A payload-range trade-off is made for every aircraft in the database, decreasing payload in steps of 10 passengers until a specified minimum is reached. For each off-design configuration the aircraft performance parameters are calculated. The combination capacity-range-runway is directly obtained from the trade-off. The performance indicators $fuel/energy\_climb\_descent$, $fuel/energy\_km$ and $max\_fuel/energy$ can be calculated from the aircraft mass build up. The aircraft cost and operating times are assumed to be the same as the original on-design aircraft.

### 2. Payload vs. Runway

Aircraft in the network can only operate a route when they can take-off and land on the smallest runway length on this route. This can also be achieved by reducing the payload that the aicraft is carrying. However, this again means that the frequency might need to be increased to meet passenger demand. In the payload-runway trade-off, required take-off length and landing length are determined for each aircraft configuration with reduced payload (limiting take-off mass).

The required take-off length is estimated using the take-off parameter (TOP) from Raymer [74], as shown in

13

Equation (33). The take-off weight $W_{TO}$ is varying for each situation as the payload mass is decreased. The wing surface area $S$, the take-off power $P$, the lift coefficient in take-off configuration $C_{L_{TO}}$ are kept the same as for the on-design aircraft. The required landing length ($S_L$) is estimated from the relation between stall speed and landing length from Roskam [58]. Equations (34) and (35) show this relation, and the calculation for stall speed. Stall speed is calculated for landing weight, $W_L$, which is also recalculated due to decreased payload mass. Maximum lift coefficient in landing configuration $C_{L_{max}}$ is assumed equal to that of the on-design aircraft.

$$TOP = \frac{W_{TO}}{S} \cdot \frac{W}{P} \cdot \frac{1}{C_{L_{TO}}} \qquad (33)$$

$$V_{S_L} = \sqrt{\frac{W_L \cdot 2}{S \cdot \rho \cdot C_{L_{max}}}} \qquad (35)$$

$$S_L = 0.5847 \cdot V_{S_L}^2 \qquad (34)$$

The required runway length is the limiting of take-off and landing distance. Similar to the payload-range diagram, a payload-runway diagram can be constructed as seen in Figures 10 and 11. A kink can be observed in the payload-runway diagram, for which the limiting condition switches from take-off to landing. Also, these payload-runway off-design aircraft configurations are added to the aircraft database.
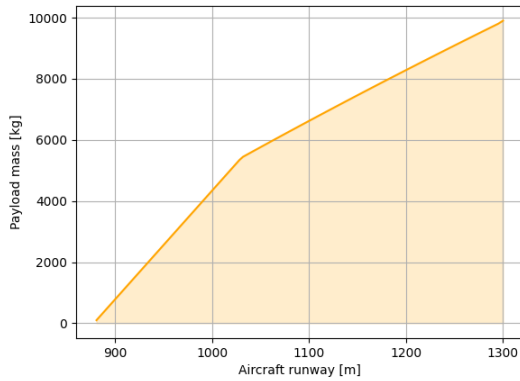


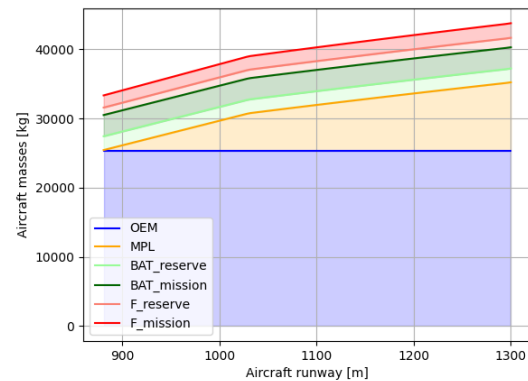**Fig. 10    Payload-runway (constant battery mass)**



**Fig. 11    Aircraft masses (constant battery mass)**

### 3. Operation-based aircraft redesign

The aircraft, together with off-design configurations, are provided as a database to the fleet-and-network allocation module with the aim to maximize airline profit. From the network allocation output, it is possible to identify how the aircraft are operated in the network. Per route, the distance and minimum airport runway length are known. Hence, it is possible to plot the routes flown in the payload-range diagram by plotting the operated aircraft capacity and the route distances flown. Each route is represented by a point in the diagram and has an associated minimum runway length of that route. An example figure can be seen in Figure 12.

Routes flown with on-design aircraft are marked with a circle (○), routes flown with a payload-range trade-off configuration are marked with a cross (×) and the ones flown with a payload-runway trade-off configuration with a triangle (△). It is important to note that this does not fully cover off-design operations, since also on-design aircraft may be selected for routes shorter than their harmonic point. This limitation is at this point not yet addressed in the model due to the MLIP approach. The network model requires aircraft to be operated at a certain load factor, hence passenger capacity points are vertically aligned. Only when a flight cannot be flown at full capacity (due to runway requirements), the point will deviate from its vertical position in the graph. From this information on the aircraft operations, new aircraft designs will be generated with a passenger capacity, aircraft range and design runway length better suited to operations in the network. This is explained in the next section.

### 4. New Aircraft Design Propositions

The network allocation determines the generation of new aircraft designs. New designs are derived from the aircraft in the database, based on exchanges between payload mass, range, and runway length. This is done in two ways: (1) a clustering method and (2) a limit-case operation analysis.
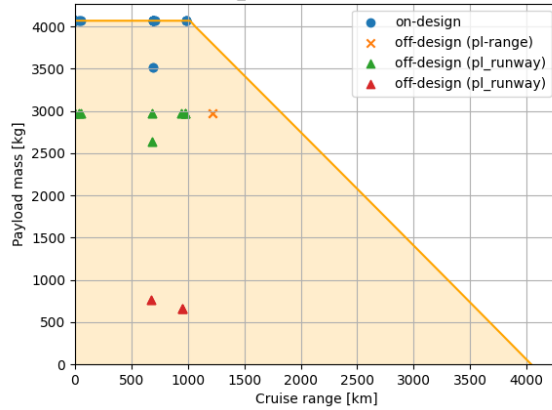
**Fig. 12    Route operations plotted in payload-range diagram**

**Clustering Method**

As could be observed from Figure 12, aircraft may be operated at ranges smaller than the range for which the aircraft was designed. Often, these operated ranges are grouped in several clusters. New aircraft designs will therefore be generated with ranges that better match operated routes based on these clusters. Considering Figure 12, a clear range clustering is observed at the payload-runway off-design configuration at payload mass ~3000 kg (or ~30 passengers) (▲). For this aircraft configuration, the operated ranges and runway lengths are shown in Table 2.

**Table 2    Distance and runway length for aircraft ▲in Figure 12 at payload 3000 kg**

| distance [km] | 31 | 51 | 970 | 680 | 680 | 940 |
|---|---|---|---|---|---|---|
| runway length [m] | 1655 | 1595 | 1342 | 1268 | 1270 | 1342 |

Starting from this identified cluster, the following steps are taken to develop a new aircraft concept:

1) Allocate the route distances to a binary array, where each bin width is defined by a specified 'split' value. For example, if a split value of 100 km is selected and the maximum route distance is 1100 km, the bins are as showed in the table below as *'Range bins [km]'*. The routes are allocated to a binary array, where *'1'* indicates the aircraft is flying on routes with distances within the range bin width. In the example, the ranges in Table 2 are colored and matched with the binary array allocation in the table below for better visualization.
2) The operational ranges are defined by the maximum range of each range interval.
3) The operational runways are defined by the minimum runway in each interval.

**Table 3    Steps 1 to 3 of clustering method, applied to aircraft ▲in Figure 12 at payload 3000 kg which is operated at the points in Table 2**

| | Range bins [km] | 0-100 | 100-200 | 200-300 | 300-400 | 400-500 | 500-600 | 600-700 | 700-800 | 800-900 | 900-1000 | 1000-1100 |
|---|---|---|---|---|---|---|---|---|---|---|---|---|
| Step 1: | Binary | 1 | | | | | | 1 | | | 1 | |
| Step 2: | Range [km] | 100 | | | | | | 700 | | | 1000 | |
| Step 3: | Runway [m] | 1595 | | | | | | 1268 | | | 1342 | |

4) The combination of consecutive intervals is defined by a 'threshold' value which specifies the minimum range between two consecutive clusters for which a new aircraft will be designed. For example, with a threshold value of 400 km, the clustering is as follows:

clustered ranges:  [100] [700, 1000]

clustered runways:  [1595] [1268, 1342]

15

5) The new aircraft will have a design range equal to the maximum range of each cluster and a design runway length equal to the minimum runway length of each cluster (with runway bins spanning 50m):

<div style="text-align:center">

aircraft 1: 30 passengers - 100 km cruise range - 1550 m runway length

aircraft 2: 30 passengers - 1000 km cruise range - 1250 m runway length

</div>

Through these five steps, the clustering method introduces new aircraft. For the above example above, two new aircraft design are created. These designs are subsequently added to the database such that they can be considered in the next fleet allocation step.

**Limit-case Operations**

Using the clustering method, operations of on- and off-design configurations are inspected and clustered together in order to make multiple, smaller aircraft that better fit the network. This does not take into account the design of aircraft with larger passenger capacities and larger operational ranges. Therefore, a limit-case operation analysis is performed where it is checked whether an aircraft is operating at its limiting conditions of maximum payload and maximum range. The following design strategy is applied to come up with additional aircraft designs:

1) *If* the aircraft operates within 5% of the harmonic design point
   ⟹ increase both the payload capacity (+10) and the design range (+split) at the same time.
2) *If* the aircraft operates at its maximum payload *or if* it operates at a payload-runway trade-off condition
   ⟹ increase the payload capacity (+10) for the same aircraft range.
3) *If* the aircraft operates within 5% of the maximum range at a given payload
   ⟹ increase the design range (+ split) for that payload capacity.

All new aircraft generated from both the clustering method and the limit-case operation analysis, have to adhere to the aircraft design constraints mentioned in Section II.B.8. Only the designs that have a converged maximum take-off weight within 0.1% with respect to the previous iteration and meet all design constraints, are added to the aircraft database and can be implemented in the next fleet allocation.

The aircraft database will grow with every iteration. Therefore, a database clear-up is performed. Only the aircraft chosen by the fleet allocation per iteration, together with their payload-range and payload-runway configurations, are kept in the database. Aircraft that are not chosen are removed. The iteration procedure will last until the fleet-and-network allocation does not select any of the newly proposed aircraft designs.

**F. Intermezzo - Aircraft Design Linearization**

Case study 1 relies on a linearization around the design point of a set of aircraft designs generated with the "Aircraft Design Initiator". This in-house developed conceptual design tool (in short, the *Initiator*) performs a design convergence over a number of disciplinary analyses and sizing methods. The work of de Vries et al. [11] on preliminary sizing methods for Distributed Hybrid Electric Propulsion (DHEP) made it possible to synthesize hybrid-electric aircraft configurations with the Initiator[75]. Additionally, a simplified surrogate model was included to quantify the effects of distributed propulsion on the wing aerodynamics. More information on the Initiator can be found in [75–77].

*1. Linearized Aircraft Variants*

The actual linearization uses variations of the range equation to provide a relation between aircraft size, payload (passenger capacity), energy capacity, and range. This equation (Breguet Range Equation) was originally established for kerosene aircraft, as presented in Equation (36). This work uses the hybrid-electric and fully electric aircraft derived by de Vries et al. [71] presented in Equations (28) and (37). Since these equations only need a set of parameters to "create" new aircraft variants, this method can be coupled with a strategic airline planning model. This way, strategic airline planning and electrified aircraft design can be integrated linearly around the original aircraft design point. Thus, this step does not carry out a complete aircraft redesign, as is the case for Case study 2, but rather provides a fast alternative to assess slightly smaller or larger aircraft by only trading-off payload and range. Here we assume that battery mass can be reduced to increase payload mass and vice-versa. This exchange is done by assuming an extra row of seats in the same airframe. It must be noted that this assumption is limited to the addition of only a single row of seats or a maximum of two rows for longer fuselages.

<div style="text-align:center">16</div>

*Breguet Range equation for kerosene aircraft:*

$$R = \eta_1 * \eta_3 * \frac{e_f}{g} * \frac{L}{D} * \ln\left(\frac{W_{OE} + W_{PL} + W_f}{W_{OE} + W_{PL}}\right) \tag{36}$$

*Range equation for fully-electric aircraft [71]:*

$$R = \eta_2 * \eta_3 * \frac{L}{D} * \frac{E_{0\_tot}}{W_{OE} + W_{PL} + W_{bat}} \tag{37}$$

*2. Network Model Extension for Linearized Aircraft Variants - Only for Case Study 1*

The trade-off between payload and range impacts the routes that can be flown. Removing one row from the aircraft extends the aircraft range. Hence, routes within this extended range can be flown with decreased capacity. On the other hand, adding one row to the aircraft reduces the aircraft range. Hence, some routes are not available anymore for aircraft with an increased capacity. To reflect this in the operations, the fleet allocation model defined in Section II.E.3 has to be updated. In the following paragraphs the differences in the MILP model are discussed to facilitate this linearized aircraft design. The objective function remains the same.

**Extra Parameters**

Performance calculations, such as presented in Equations (4) to (9), should be defined for new aircraft variants to define which routes can be flown with which variant. This leads to two additional parameters $AR\_less$ and $AR\_extra$:

- $AR\_less_k^r$, this equals 1 if route $r$ can only be flown by aircraft $k$ when having one less row
- $AR\_extra_k^r$, this equals 10000 if route $r$ can be flown by aircraft $k$ when having one extra row

**Extra Decision Variables**

The following decision variables are added to be able to vary between the aircraft with additional or fewer rows:

- $extra\_row_k^r$ : one row is added for all frequencies of aircraft type $k$ on route $r$
- $less\_row_k^r$ : one row is removed for all frequencies of aircraft type $k$ on route $r$
- $row\_0_k^r$ : no row changes for all frequencies of aircraft type $k$ on route $r$
- $extra\_row\_binary_k^r$ : binary value of $extra\_row_k^r$
- $less\_row\_binary_k^r$ : binary value of $less\_row_k^r$
- $row\_0\_binary_k^r$ : binary value of $row\_0_k^r$

**Extra Constraints**

Set of constraints Equation (38): flow from airport $i$ to $j$ on route $r$ should be less or equal to the total seats on aircraft flying from airport $i$ to $j$ on route $r$

$$\sum_{a\in N}\sum_{b\in N}\left[x_{a,b}^r * R3_{a,b_{i,j}}^r + \sum_m w_{a,b}^{r,m} * R3_{a,end_{r_{i,j}}}^r * R4_{a,b}^{r,m} + \sum_m w_{a,b}^{m,r} * R3_{start_r,b_{i,j}}^r * R4_{a,b}^{m,r}\right]$$
$$\leq \sum_k R1_{i,j}^r * \left(z_k^r * seats_k + \left(extra\_row_k^r - less\_row_k^r\right) * seats\_per\_row_k\right) * LF \tag{38}$$
$$\forall r \in \boldsymbol{R}, i, j \in N$$

A set of constraints Equation (39) is added to make sure that if a route can only be flown by an aircraft variant with one less row, this variation is chosen.

$$z_k^r \leq less\_row_k^r \qquad \forall r, k \in AR\_less_k^r = 1 \tag{39}$$

Complementary to the previous constraint, the set of constraints Equation (40) is added to ensure that an extra row can only be added if the aircraft can still fly this route.

$$extra\_rows_k^r \leq AR\_extra_k^r \qquad \forall k \in \boldsymbol{K}, r \in \boldsymbol{R} \tag{40}$$

To guarantee that the same aircraft variant is chosen for every frequency per aircraft type per route, a set of constraints Equations (41) to (45) is added to the model. This set of constraints highlights the need for the six additional decision

decision introduced abooove: a binary variant of both decision variables *extra_row* and *less_row*, and a variable to state no change in rows: *row_0* and its binary variant are required. The factor $M$ is a large number, much higher than the highest expected frequency per route (z) and the number of aircraft in the fleet (ac).

$$extra\_row\_binary_k^r + less\_row\_binary_k^r + row\_0\_binary_k^r = 1 \qquad \forall k \in K, r \in R \qquad (41)$$

$$extra\_row_k^r + less\_row_k^r + row\_0_k^r = z_k^r \qquad \forall k \in K, r \in R \qquad (42)$$

$$extra\_row_k^r \leq M * extra\_row\_binary_k^r \qquad \forall k \in K, r \in R \qquad (43)$$

$$less\_row_k^r \leq M * less\_row\_binary_k^r \qquad \forall k \in K, r \in R \qquad (44)$$

$$row\_0_k^r \leq M * row\_0\_binary_k^r \qquad \forall k \in K, r \in R \qquad (45)$$

The result of the extended LP model presents aircraft variants that enhance the network performance. It indicates which aircraft variant is profitable per aircraft type per route.

## III. Verification and Validation

This section summarizes the verification and validation steps which were performed on the aircraft design approach and the fleet allocation model. Section III.A studies the design of a conventional to validate the design approach. Additionally, results of the hybrid-electric aircraft design are compared to those presented by Finger et al. [78, 79]. In Section III.C, we introduce the reference network to which the case studies will compared. This reference network also allows us to verify the working principle of the fleet allocation model.

### A. Validation of Conventional Aircraft Design

The conventional aircraft design method has been validated against the Dash 8 Q400 aircraft, using the data listed in the Q400 Fuel Efficiency Manual[f]. To simulate this aircraft, we assumed a payload of 80 passengers, resulting in a total payload mass of 8489 kg. The mission consists of three main mission segments: a cruise stage of 500 nmi (at 23000 ft and 182 m/s), diversion of 100 nmi (at 5000 ft and 182 m/s), and loiter of 45 minutes at 1500 ft. The aircraft is sized to have a take-off distance of 1300 m and a stall speed of 47.15 m/s. The configuration features a high-wing installation with T-tail and undercarriage stored in the nacelles. The wing has an aspect ratio of 12.8. The gas turbine engines have an efficiency of 34% (propulsive efficiency during cruise 0.8, propulsive efficiency during endurance 0.77 (from statistics)). The results of this validation are presented in Table 4. Based on these results, we consider the aircraft design approach validated for kerosene, regional, turboprop-powered aircraft.

**Table 4    Comparison of model output versus aircraft data for Q400**

| Parameter | Unit | Result | Reference | Difference |
|---|---|---|---|---|
| OEM | $t$ | 18.0 | 17.8 | +0.8% |
| MTOM | $t$ | 29.7 | 29.6 | +0.6% |
| PLM | $t$ | 8.49 | 8.49 | 0.0% |
| FM | $t$ | 3.30 | 3.27 | +1.1% |
| Take-off fuel | $kg$ | 41.6 | 42.0 | +1.0% |
| Climb fuel | $kg$ | 325 | 324 | +0.2% |
| Cruise fuel | $t$ | 1.32 | 1.34 | -0.9% |
| Descent fuel | $kg$ | 319 | 318 | +0.3% |
| Reserve fuel | $t$ | 1.29 | 1.23 | +5.3% |
| Wing area | $m^2$ | 63.5 | 63.1 | +0.5% |
| Wingspan | $m$ | 28.5 | 28.4 | +0.4% |

---

[f]Data from Bombardier Q400 Fuel Efficiency Manual

**B. Verification of a Parallel Hybrid-Electric Dornier 228**

A comparison to Finger et al. [78, 79] is made by designing a parallel hybrid Dornier 228. The verification procedure focuses on correct usage of the powertrain matrix, comparing aircraft-level and component-level power-loading diagrams. The power-loading diagrams are constructed for the following constraints from [78]:

- Cruise speed constraint: 115 m/s at 3000m with $\eta_P$ of 80%;
- Take-off length constraint: take-off distance 793 m at sea level;
- Stall speed constraint: 34.6 m/s at sea level;
- Climb rate constraint in all-engines-operative condition (AEO): 8 m/s with $\eta_P$ of 70%;
- Climb rate constraint in one-engine-inoperative condition (OEI): 2m/s with $\eta_P$ of 65%.

It should be noted that the paper by [79] makes use of a two term drag polar (Equation 46), while the aerodynamics module presented in this work makes use of a symmetric drag polar (Equation 47). The symmetric aerodynamic drag values are obtained by matching the drag polar as close as possible to the two term drag polar, however, this causes a slight error in drag estimation for validating the results. In the model we estimate a zero-lift drag coefficient $C_{D_0}$ of 0.025, an Oswald efficiency factor $e$ of 0.8, and a maximum lift coefficient $C_{L_{max}}$ of 1.7 in clean configuration.

$$C_D = C_{D,min} + \frac{(C_L - C_{L,minD})^2}{\pi A e} \tag{46}$$

$$C_D = C_{D_0} + \frac{C_L^2}{\pi A e} \tag{47}$$

The aircraft-level, gas turbine and primary electric motor power-loading diagrams are compared to those from Finger et al. [78]. These diagrams are shown in Figures 13 to 15, respectively. The results are summarized in Table 5 and show that the module is able to generate the correct power-loading diagrams and determine the correct design point. There is a slight offset attributed to the different drag polars.

**Table 5    Verification Power-Loading Diagram Results Hybrid Dornier 228**

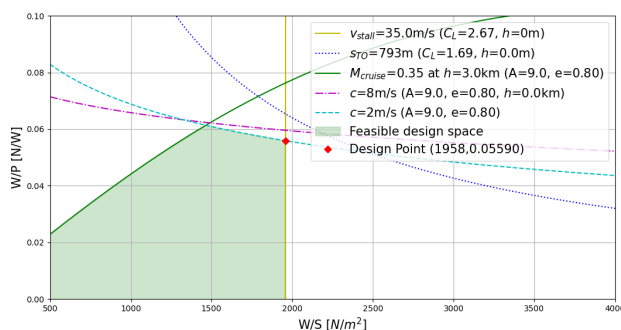|  | Unit | Result | Finger et al. [78] | Sizing constraint |
|---|---|---|---|---|
| Aircraft Design Point (W/S; P/W) | $N/m^2; W/N$ | 1958; 17.9 | 1958; 17.9 | OEI rate of climb |
| Gas Turbine Design Point (W/S; P/W) | $N/m^2; W/N$ | 1958; 16.8 | 1958; 16.8 | AEO rate of climb |
| Electric Motor Design Point (W/S; P/W) | $N/m^2; W/N$ | 1958; 1.80 | 1958; 1.78 | OEI rate of climb |
| Gas Turbine Mass | $kg$ | 318 | 317 | - |
| Electric Motor Mass | $kg$ | 19.0 | 18.9 | - |



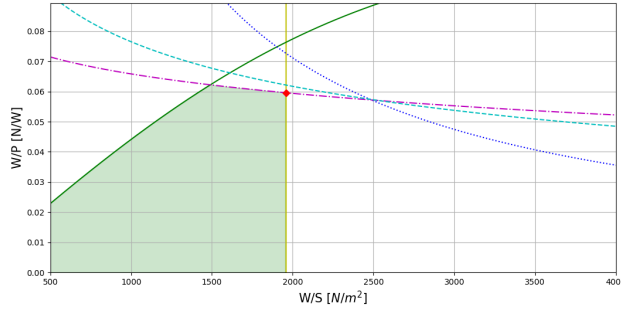**Fig. 13    Aircraft-level power-loading diagram**

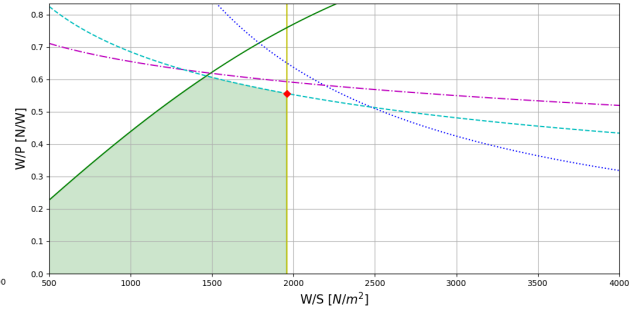**Fig. 14    Gas Turbine power-loading diagram**



**Fig. 15    Electric Motor power-loading diagram**

Additionally, the energy analysis module is validated by comparing the fuel mass and energy mass required to perform the mission as defined by Finger et al. [78] consisting of a cruise phase of 396 km range (at 3000 m and 115 m/s), diversion of 270 km (at 1000 m and 85 m/s), and loiter of 30 minutes (at 450 m). The results of the energy analysis are summarized in Table 6 and show a maximum difference of 3.5% in the weight prediction of the fuel weight.

**Table 6    Energy analysis hybrid Dornier 228**

| Parameter | Unit | Result | Finger et al. [78] | Difference |
|-----------|------|--------|--------------------|-----------|
| Fuel mass | $kg$ | 498 | 481 | +3.5% |
| Battery mass | $kg$ | 117 | 115 | +1.7% |

### C. Strategic Airline Planning Reference Case

The network-and-fleet model has been validated against a baseline scenario for a small European regional airline, provided by SATA Air Açores. This comparison uses a database with the current operational fleet of aircraft to determine whether the model produces similar fleet and network planning. The serviced airports are reported in Table 7, average demand data cannot be shared due to confidentiality. The network is currently served by Bombardier Dash 8 Q400 and Q200 aircraft. The design tool is used to generate aircraft according to the set of inputs provided in Table 8.

**Table 7    SATA Air Açores airports**

| Location | IATA code | ICAO code | Refueling facility | Runway length |
|----------|-----------|-----------|--------------------|---------------|
| Santa Maria | SMA | LPAZ | Yes | 3048 m |
| San Miguel - Ponta Delgada | PDL | LPPD | Yes | 2323 m |
| Terceira | TER | LPLA | Yes | 3310 m |
| Graciosa | GRW | LPGR | No | 1268 m |
| São Jorge | SJZ | LPSJ | No | 1270 m |
| Pico | PIX | LPPI | Yes | 1655 m |
| Faial – Horta | HOR | LPHR | Yes | 1595 m |
| Flores | FLW | LPFL | No | 1342 m |
| Corvo | CVU | LPCR | No | 761 m |

The network model is run to maximize airline profit, using an average weekly passenger demand and public service obligations. The maximum operating time of the aircraft per day is estimated at 9.35 hours. Each route consists of a maximum of two subsequent flights. Each flight is occupied at 85% of maximum aircraft capacity (load factor 0.85).

The results of the fleet-and-network allocation show a total fleet size of five aircraft is required, consisting of two Q400 and three Q200, as shown in Table 9. In reality however, the fleet consists of six aircraft: four Q400 and two

20

**Table 8    Design inputs for kerosene reference aircraft**

| Parameter | Unit | Dash 8 Q400 | Dash 8 Q200 |
|---|---|---|---|
| Harmonic cruise range | k$m$ | 926 | 1020 |
| Passenger capacity | – | 80 | 37 |
| Cruise altitude | $m$ | 7010 | 7600 |
| Cruise velocity | $m/s$ | 182 | 150 |
| Take-off distance | $m$ | 1300 | 1000 |
| Aspect ratio | – | 12.8 | 12.3 |
| Payload mass | $kg$ | 8489 | 4200 |
| Max fuel mass | $kg$ | 5300 | 2500 |

Q200. The difference can be attributed to the simplifications and assumptions. Additionally, the amount of available seat kilometers may not be the same due to the employed assumptions and the greediness of the optimizer in trying to maximize profit.

The Q400 operates high demand routes (PDL-TER, PDL-HOR, PDL-PIX, PDL-SMA). However, a reduced payload mass must be used to meet the minimum runway requirement of 1300m, for GRW, SJZ and CVU airports. The off-design configuration is operated on routes which can include an additional stop, but it does not service the highest demand route and the CVU airport can still not be serviced. Two Q200 aircraft are operating at maximum passenger capacity, and one is operated at lower passenger capacity to service also the CVU airport. The off-design configuration is typically covering long distance routes instead of single flights as there is no fueling facility at CVU.

**Table 9    Baseline kerosine fleet; aircraft reported as (passengers - total range [km] - runway length [m])**

| Aircraft | On design configurations | Off design configurations |
|---|---|---|
| Q400 | 1x Q400$_{on}$ (80-1135-1300) | 1x Q400$_{off}$ (70-1135-1252) |
| Q200 | 2x Q200$_{on}$ (37-1246-1000) | 1x Q200$_{off}$ (17-1246-755) |

## IV. Case Study 1:  Regional Airline Network

This case study presents the results for the linearization approach around the aircraft design point, using a pre-defined set of hybrid-electric, fully-electric, and kerosene-fueled aircraft, as shown in Table 10. Please note that very optimistic battery technology scenarios are assumed. However, the point is to study the effect on an airline network in the hypothetical case in which these aircraft would exist. It is important to note that due to this simplified approach, for case study 1, only cruise performance is used in the strategic airline model and that landing, and take-off (LTO) emissions are not realistically accounted for. This linearized model around the selected design point, trades payload for energy as described in Section II.F. Case study 1 provides the starting point for the investigation with the coupling approach that was introduced in Section II.A of case study 2. Thanks to its simplicity, case study 1 allows investigating effects of fleet composition (electric, hybrid-electric and kerosene aircraft), as well as $CO_2$ taxation.

The linearization approach evaluates aircraft variants for aircraft in the database to identify better fits with the network. Therefore, aircraft limitations for a maximum number of seats should be considered. For the presented database, the maximum addition of seats is one row for aircraft up to 48 seats and two rows of seats for larger aircraft. The number of rows can always decrease until no more seats are left. Figure 16 and Figure 17 show the outcomes for a study on a regional airline network. The absolute numeric values are anonymized in this work for confidentiality reasons.

Figure 16 illustrates the different fleet compositions and relation to profit and $CO_2$. For now, only in-flight emissions are considered. This assumption explains the zero emissions for fully electric aircraft. The results for emissions are as one would expect, but it is interesting to see that combined fleets are actually able to perform better in terms of profit and $CO_2$. This occurs both for FE, HE and KE versus KE only, and FE plus HE versus HE only. This seems to be

**Table 10    Initial aircraft database for case study 1**

| | | | | | |
|---|---|---|---|---|---|
| **Fully-electric** | **FE20**: 20 seats, 400 km range, $e_b$ = 500 Whr/kg | **FE28**: 28 seats, 1036 km range, $e_b$ = 700 Whr/kg | **FE48**: 48 seats, 1000 km range, $e_b$ = 700 Whr/kg | | |
| **Hybrid-electric** | **HE20**: 20 seats, 400 km range, $e_b$ = 500 Whr/kg | **HE28**: 28 seats, 1036 km range, $e_b$ = 500 Whr/kg | **HEA48**: 48 seats, 1000 km range, $e_b$ = 500 Whr/kg | **HEB48**: 48 seats, 1302 km range, $e_b$ = 700 Whr/kg | **HE70**: 70 seats, 1530 km range, $e_b$ = 700 Whr/kg |
| **Kerosene** | | | **Q200**: 37 seats, 1839 km range | | **Q400**: 80 seats, 2656 km range |
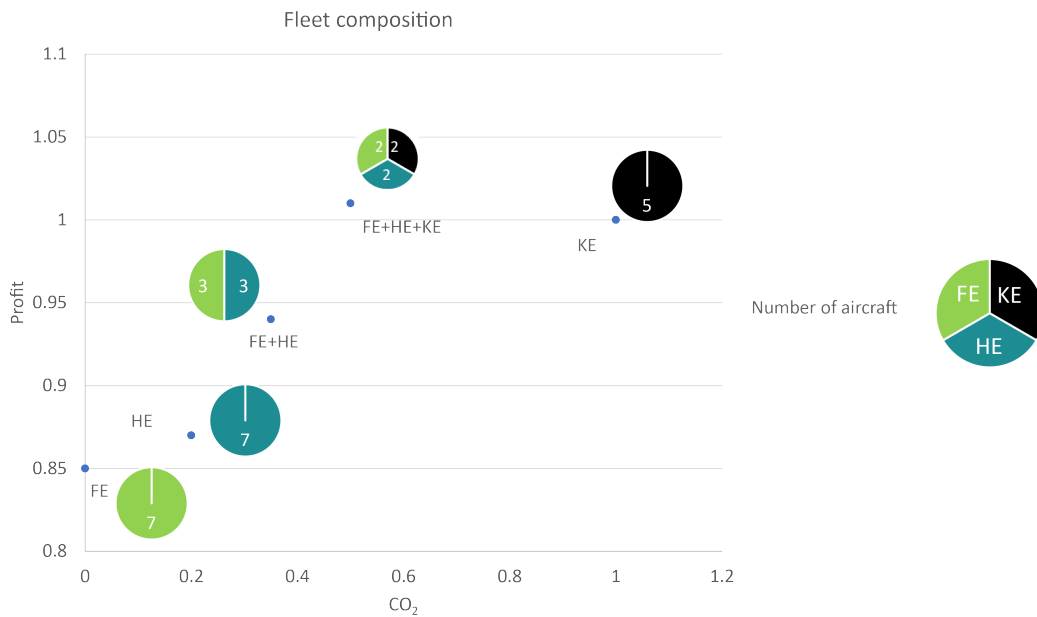


**Fig. 16    Illustration of results for the current operating environment**

caused by lower operational costs yet increased ownership costs. However, it should be noted that also the available fleet kilometers have reduced by 11% in comparison to the only kerosene-fueled case. This naturally impacts the total emissions. Additionally, not only those aircraft with the most optimistic battery technology scenario are chosen due to the associated cost penalty. The selected aircraft for each fleet are specified in Table 11, where +1 and +2 indicate whether the aircraft has been resized by adding one or two rows (only allowed for the largest aircraft). Generally speaking, the optimizer tries to increase the capacity of the smaller aircraft due to their ability to serve all the routes in the network.

For the different aircraft, it is also seen that the model tries to extend aircraft capacity to transport more passengers and be more profitable over routes with the large, required capacity. In most cases, this seems to be dictated by the various cost components (ownership and operating cost per seat) rather than operational flexibility.

Different scenarios for $CO_2$ emission taxation are presented in Figure 17. In terms of aircraft designs, only the smallest aircraft (FE and the smallest HE) are increased in payload capacity, as the algorithm is clearly favouring smaller $CO_2$ impact. Interestingly, only the high $CO_2$ taxes of cases D, E and F start to have an impact on both profit and emissions. In fact, A, B and C use the same fleet of aircraft, whereas between D and E a fully electric aircraft replaces a hybrid-electric one of the same capacity as can be seen in the resulting aircraft database for this study in Table 12. None of the $CO_2$ tax levels is forcing the optimizer to not use any kerosene aircraft (or hybrid) and consequently the fleet still emits around 40% of the original amount of $CO_2$ due to the optimizer favouring flights profit over $CO_2$ emissions.

Two additional studies, H and I, are included in Table 12. These studies show the fleet composition in case the price of electric energy is halved (H) and the kerosene price is doubled (I). Interestingly, scenario I does not see a change in fleet

composition and hence no change in CO2 emissions. Only the profit is negatively impacted, moving to around 95% of the baseline. For scenario H, emissions are sligthly impacted due to the use of an FE28+1 aircraft instead of an HE28+1. Profit is slightly increased above the baseline situation (O).

**Table 11    Aircraft database for current operating environment**

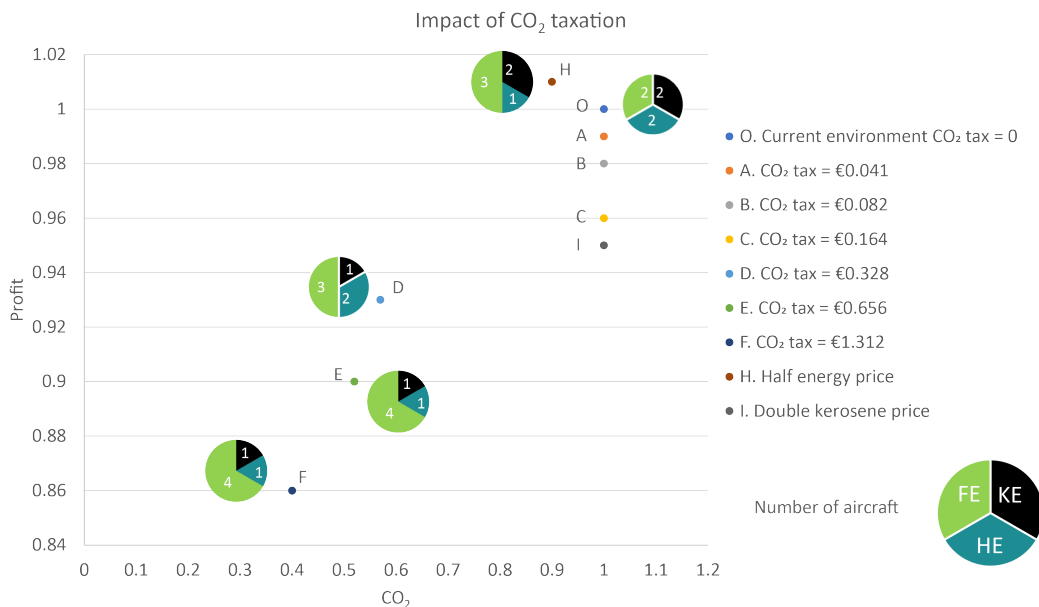| KE | | | Q200: 3 | | Q400: 2 |
|---|---|---|---|---|---|
| **FE** | **FE20+1**: 1<br>$e_b$ = 500 Whr/kg | **FE28+1**: 2<br>$e_b$ = 700 Whr/kg | **FE48+1**: 4<br>$e_b$ = 700 Whr/kg | | |
| **HE** | **HE20**: 1<br>$e_b$ = 500 Whr/kg | **HE28+1**: 2<br>$e_b$ = 500 Whr/kg | **HEA48**: 1<br>$e_b$ = 500 Whr/kg | **HEB48**: 1<br>$e_b$ = 700 Whr/kg | **HE70+2**: 2<br>$e_b$ = 700 Whr/kg |
| **FE+HE** | | **HE28+1**: 1<br>$e_b$ = 500 Whr/kg | **FE48+1**: 3<br>$e_b$ = 700 Whr/kg | **HEB48**: 1<br>$e_b$ = 700 Whr/kg | **HE70+2**: 1<br>$e_b$ = 700 Whr/kg |
| **FE+HE+KE** | **FE20+1**: 2<br>$e_b$ = 500 Whr/kg | **HE28+1**: 1<br>$e_b$ = 500 Whr/kg | **HEB48**: 1<br>$e_b$ = 700 Whr/kg | | Q400: 2 |



**Fig. 17    Illustration of results for an operating environment with $CO_2$ tax**

**Table 12    Aircraft database for current operating environment**

| O,A,B,C,I | FE20+1: 2<br>$e_b$ = 500 Whr/kg | HE28+1: 1<br>$e_b$ = 500 Whr/kg | | HEB48: 1<br>$e_b$ = 700 Whr/kg | Q400: 2 |
|---|---|---|---|---|---|
| **D** | FE20+1: 1<br>$e_b$ = 500 Whr/kg | HE28+1: 1<br>$e_b$ = 500 Whr/kg | FE48+1: 2<br>$e_b$ = 700 Whr/kg | HEB48: 1<br>$e_b$ = 700 Whr/kg | Q400: 1 |
| **E** | FE20+1: 1<br>$e_b$ = 500 Whr/kg | FE28+1: 1<br>$e_b$ = 700 Whr/kg | FE48+1: 2<br>$e_b$ = 700 Whr/kg | HEB48: 1<br>$e_b$ = 700 Whr/kg | Q400: 1 |
| **F** | | FE28+1: 1<br>$e_b$ = 700 Whr/kg | FE48+1: 3<br>$e_b$ = 700 Whr/kg | HEB48: 1<br>$e_b$ = 700 Whr/kg | Q400: 1 |
| **H** | FE20+1: 2<br>$e_b$ = 500 Whr/kg | FE28+1: 1<br>$e_b$ = 700 Whr/kg | | HEB48: 1<br>$e_b$ = 700 Whr/kg | Q400: 2 |

23

# V. Case Study 2: Coupled Aircraft Design and Network Planning

This case study uses the same network from Section IV, however, it uses the coupling approach between aircraft design, climate optimization and strategic airline planning as outlined in Figure 1 and described in Section II.A. All hybrid-electric aircraft are designed with powertrain component properties for the 2035 time frame. The values for battery, electric motor, and converter performance are taken from de Vries [65]. The nine performed case studies are:

- A. Kerosene: This case mirrors the current situation, where the network is operated with two types of kerosene turboprops. This case is used as a reference and further results will be compared with respect to this reference case.
- B. Initial hybrid: This case study presents a first attempt to hybridize the current airline fleet by replacing the existing kerosene aircraft by hybrid-electric alternatives with similar characteristics (payload, range, runway, etc.).
- C. Design Case: A complete redesigned fleet of hybrid-electric aircraft is introduced in the network. All aircraft have a battery technology level with a specific energy of 500 $Wh/kg$ and no limits are posed on the amount of different aircraft types (fleet diversity).
- D. Climate Optimized: The aircraft of the design case are optimized to limit the climate impact by varying the cruise altitude, velocity and degree of hybridization (characterized by the power split). The optimized aircraft are introduced to the network without changing the allocation.
- E., F. Sensitivity study - technology: These cases represent a sensitivity study on the battery technology level. The battery specific energy is increased to 700 $Wh/kg$ and 1000 $Wh/kg$ in the design case.
- G., H., I Sensitivity study - diversity: Similarly, a sensitivity study is performed on the maximum fleet diversity. Fleet diversity is limited to 2, 3 and 4 aircraft in the design case.

## A. Baseline Kerosene Design Case

The overview of the results of the different case studies in terms of airline cost, profit, total network emissions and fleet composition is given in Table 13. For comparison, the results reference case A are compared to those obtained in case study 1 (Section IV). In both cases, fleet size is equal to 5 and fleet diversity is equal to 2. The ownership cost are not changed, however a change of 8% in the operating cost occurs due to the difference in modeling the amount fuel and battery energy required for a route stop. Case study 1 only includes the fuel and battery energy required to perform the take-off and landing but does not model the climb and descent phases explicitly. The differences in cost cause a slight offset in the airline profit value of 5%. Another remarkable difference can be observed in the total network emissions (38% lower in case study 1). This difference can be attributed to LTO cycle modelling, as well as case study 2 including the $CO_2$ emissions for fuel burn in-flight, fuel production on ground, and electricity production on ground.

## B. Initial Hybrid Fleet

Two parallel hybrid-electric aircraft are designed based on the Q400 and Q200 aircraft. Inputs and top-level aircraft requirements are provided in the appendix in Table 15. The results of the hybrid-electric aircraft sizing configurations are listed the appendix, in Table 16. Fleet allocation results show a total fleet size of 7 aircraft. One additional HE Q400$_{on}$ and one additional HE Q200$_{on}$ aircraft are required. The main reason is the increase in operating times to operate hybrid-electric aircraft when compared to kerosene aircraft due to the extra time required to swap the battery.

The *HE* Q400 aircraft is operated both at maximum capacity (HE Q400$_{on}$) and lower payload for increased range (HE Q400$_{off}$). The HE Q200 aircraft is operated at maximum capacity (HE Q200$_{on}$) and a payload-runway trade-off (HE Q200$_{off}$). Passengers are traded to enable taking off from the CVU airport, due to a significant increase in take-off weight passenger, the capacity has to be reduced to only 7 passengers. Consequently, the frequency of these routes has increased. The resulting fleet is summarized in Table 14. Results are summarized in Table 13. Due to the increased amount of aircraft and increased frequency, both operating (16%) and ownership (42%) cost have increased. These consequently reduced profit by 27%. The reduction in emissions from operating hybrid-electric aircraft is offset by the larger fleet and increased frequency.

## C. Redesigned Hybrid Fleet

Based on the fleet-and-network allocations, new hybrid-electric aircraft can be designed using the clustering method and the limit-case operations analysis. Figure 18 visualizes the chosen airline fleet. Each aircraft type is represented by a name, color, and its payload-range-runway combination. When one aircraft is operated at multiple configurations (on-design and off-design), the aircraft are shown in the same color and connected through a vertical line. The amount

**Table 13    Overview of network performance for all case studies**

| Case Description | Operating cost | Ownership cost | Profit | Emissions | Fleet size | Fleet diversity |
|---|---|---|---|---|---|---|
| A. Kerosene | ref | ref | ref | ref | 5 | 2 |
| Case-study 1 - Linearized kerosene only cruise performance | +8% | 0% | -5% | -38% | 5 | 2 |
| B. Initial hybrid | +16% | +42% | -27% | +0% | 7 | 2 |
| C. Design Case no max diversity, 500 Wh/kg | +8% | +10% | -13% | -11% | 6 | 6 |
| Case-study 1 - Linearized HE only cruise performance | +8% | +11% | -18% | -78% | 7 | 5 |
| D. Climate optimized design case | +9% | +10% | -14% | -38% | 6 | 6 |
| E. Sensitivity study - technology no max diversity, 700 Wh/kg | +7% | +10% | -12% | -17% | 6 | 6 |
| F. Sensitivity study - technology no max diversity, 1000 Wh/kg | +7% | +10% | -11% | -21% | 6 | 6 |
| G. Sensitivity study - diversity 2 max diversity, 500 Wh/kg | +13% | +18% | -19% | +1% | 6 | 2 |
| H. Sensitivity study - diversity 3 max diversity, 500 Wh/kg | +11% | +12% | -16% | -7% | 6 | 3 |
| I. Sensitivity study - diversity 4 max diversity, 500 Wh/kg | +9% | +12% | -14% | -6% | 6 | 4 |

**Table 14    Resulting fleet - Initial hybrid case**

| Aircraft | Configurations (passengers - total range [km] - runway length [m]) |
|---|---|
| HE Q400 | 2x HE Q400$_{on}$ (80-1109-1300) <br> 1x HE Q400$_{off}$ (70-1483-1258) |
| HE Q200 | 3x HE Q200$_{on}$ (37-1226-1000) <br> 1x HE Q200$_{off}$ (7-1226-731) |

of aircraft needed from a certain type or configuration is denoted by the number in the upper right corner. When an aircraft goes through a redesign, a new aircraft is generated, and the name gets an additional term $R_x$ where $x$ denotes the amount of redesign cycles it has gone through. A redesign cycle is marked with a red arrow. Whenever an aircraft is chosen without the need of a redesign, it is marked with a green arrow. The aircraft in the final hybrid electric fleet, with their performance indicators, are shown in Table 17.

The resulting network performance is summarized in Table 13. Compared to the initial hybrid case, a significant decrease in ownership cost can be observed (though still more than the reference scenario). This is caused by the decreased fleet size, but also due to the fleet allocation exploiting the fact that the fleet consists of smaller aircraft and the cost are a function of the number of seats. This indicates a shortcoming of the method presented: a higher fleet diversity can lead to lower airline cost while in reality a more standardized fleet is accompanied by lower cost of operations and maintenance. The higher fleet diversity allows the aircraft to be allocated more efficiently in the network and thus lowers the total network emissions by 11%. When comparing the final hybrid-electric fleet with the reference kerosene fleet, a total decrease in emissions of 11% can be obtained at the cost of a decrease in profit of 13%. This is in line with the
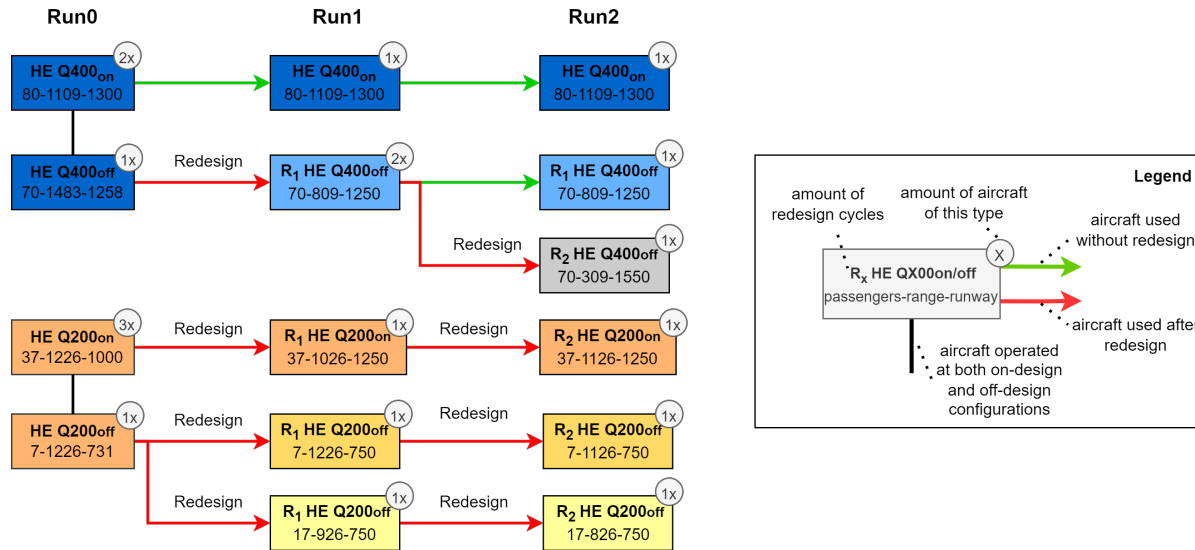
**Run0**  **Run1**  **Run2**

HE Q400$_{on}$ 80-1109-1300 (2x) → HE Q400$_{on}$ 80-1109-1300 (1x) → HE Q400$_{on}$ 80-1109-1300 (1x)

HE Q400$_{off}$ 70-1483-1258 (1x) — Redesign → $R_1$ HE Q400$_{off}$ 70-809-1250 (2x) → $R_1$ HE Q400$_{off}$ 70-809-1250 (1x)

Redesign → $R_2$ HE Q400$_{off}$ 70-309-1550 (1x)

HE Q200$_{on}$ 37-1226-1000 (3x) — Redesign → $R_1$ HE Q200$_{on}$ 37-1026-1250 (1x) — Redesign → $R_2$ HE Q200$_{on}$ 37-1126-1250 (1x)

HE Q200$_{off}$ 7-1226-731 (1x) — Redesign → $R_1$ HE Q200$_{off}$ 7-1226-750 (1x) — Redesign → $R_2$ HE Q200$_{off}$ 7-1126-750 (1x)

Redesign → $R_1$ HE Q200$_{off}$ 17-926-750 (1x) — Redesign → $R_2$ HE Q200$_{off}$ 17-826-750 (1x)

**Legend**
amount of redesign cycles; amount of aircraft of this type
$R_x$ HE QX00on/off passengers-range-runway
aircraft operated at both on-design and off-design configurations
aircraft used without redesign
aircraft used after redesign

**Fig. 18    Schematic of aircraft redesign cycle**

linearized hybrid electric case study from Section IV, except for the exaggerated difference in emissions due to the aforementioned different energy consumption, LTO cycle modeling, and inclusion of $CO_2$ emissions during production of energy. However, part of this difference is also due to the selected hybrid electric aircraft and their different battery technology scenarios.

### D. Climate-Optimized Hybrid Fleet

The climate optimization model varies, for each selected aircraft, the cruise altitude, velocity, and power split to obtain operating conditions that are minimizing the $CO_2$ emissions. Optimized aircraft results can be found in the appendix in Table 18. All climate optimized aircraft operate at lower altitudes and velocities. For aircraft with high passenger capacity and large ranges, the power split value remains practically unchanged. When lowering the capacity, the aircraft is lighter and thus benefits from a larger degree of hybridization.

The aircraft are introduced in the fleet-and-network model, without altering the fleet allocation. The results on the network performance are once more summarized in Table 13. With respect to the non-optimized aircraft, ownership cost remain the same. Operating cost increase by 1%, due to increased operational time (lower cruise speed). However, this increase in cost is offset by a decrease in fuel and energy cost. Compared to reference allocation, total emissions can be reduced by -38% at the cost of a profit decrease of -14%.

When aircraft are optimized for climate impact, the constraint line for the cruise speed in the power-loading diagram will be altered, which might affect the chosen design point. All but one of the non-optimized aircraft were originally sized by the take-off length and stall speed constraint, with one exception: the *On_design* 70-1126-750. This aircraft is sized by the cruise speed constraint, while the optimized aircraft is sized by the take-off length constraint. Figure 19 shows the aircraft power-loading diagram with the cruise speed constraint before optimization, after optimization (combined effect of Φ, *V* and *h*) and the effect of the individual parameters.

On aircraft-level, there is no effect of power split value, lowering the cruise altitude only has an effect at larger wing-loading values and lower cruise velocity has the largest effect and increases the power-loading value at all wing-loading values. This results in an increase of the feasible design space, with larger power-loading values when compared to the non-optimized aircraft. While the limiting constraint switches from cruise-speed (non-optimized) to take-off length (optimized), the value of the design point is changed only minimally.

The gas turbine power-loading diagram and electric motor power-loading diagram are depicted in Figure 20 and Figure 21 respectively. Increasing the power split value results in a higher degree of hybridization and such, the gas turbine requires less power, increasing the power-loading values. The opposite is true for the electric motor, which requires more power and therefore the power-loading is decreased. The effect on the electric motor is more pronounced.
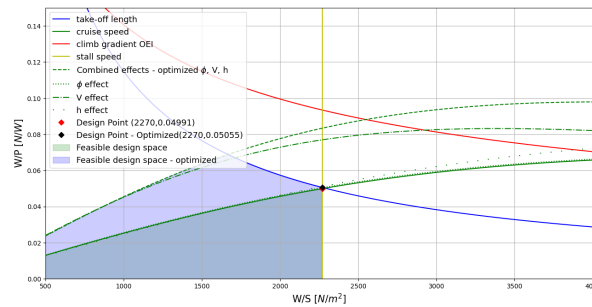
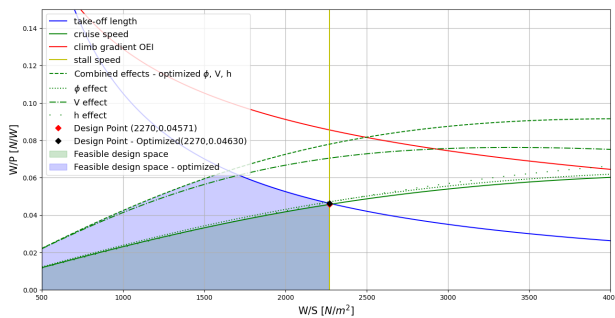**Fig. 19    Climate-optimized aircraft-level power-loading diagram**



**Fig. 20    Climate-optimized Gas Turbine power-loading diagram**



**Fig. 21    Climate-optimized Electric Motor power-loading diagram**

### E. Sensitivity Studies

Sensitivity studies are performed for battery technology scenario, increasing specific energy to 700 and 1000 $Wh/kg$, as well as maximum fleet diversity. Results are summarized in Table 13, Figures 22 and 23 in the appendix illustrate fleet compositions for the redesign cycles. The effects on emissions are larger than the effects on airline profit for battery technology scenarios. In terms of emissions, the largest emission decrease is still achieved by a climate optimization. Changing the battery technology only shows a limited effect on the final fleet composition. Limiting fleet diversity trades profit increase for increased emissions.

## VI. Conclusion

This paper presented a coupling approach for the direct integration of (hybrid-) electric aircraft design and strategic airline planning, the latter involving both fleet and network planning. An initial case study has been presented with a database of initial aircraft that can be linearly modified around their design point. These results, on a case study with a regional airline network, illustrate the effects of $CO_2$ taxation and fleet selection on profit and emissions. Results indicate that only for a relatively high $CO_2$ tax an impact on the fleet diversity can be seen. Additionally, the introduction of hybrid and electric aircraft in a fleet has shown potential for a profit increase with $CO_2$ emission reduction, at the cost of fewer available fleet kilometers.

For the coupled design, strategic airline planning and climate optimization approach, case studies were performed to understand the impact of considering airline fleet-and-network allocation integrated with hybrid-electric aircraft design and climate optimization, in terms of airline profitability, expected climate impact, and optimal aircraft design. Typically, airline cost are increased when operating hybrid-electric aircraft. This is mainly due to increased operating time of hybrid-electric aircraft as the turnaround time increases. The effect of increased turnaround time is twofold: it causes an increase in operating cost and it requires the fleet to be larger. The fleet size increases ownership cost.

Furthermore, hybrid-electric alternatives tend to have an increased weight. In order to take-off/land from the same runway length, the aircraft can take less payload onboard, which in turn increases the flight frequency of the aircraft to achieve the same passenger demand. Having to fly more often also negatively influences the aircraft cost. This leads to the fact that in terms of airline profitability, operating the kerosene fleet is the most profitable option for the airline.

The design case (case C.) demonstrates potential to decrease emissions with respect a kerosene fleet by 11% when a

hybrid-electric fleet is designed particularly for the specified network. However, this comes at the penalty of a profit reduction of 13%. The decrease in emissions can be partially attributed to higher fleet diversity with more electrified aircraft. Limiting fleet diversity to 3 types (case H.) lowers the emissions by only 7%. Battery technology levels have a notable effect on the total network emissions; however, it does not significantly impact the fleet composition. Increasing the battery specific energy shows an expected beneficial effect on emissions. The largest emission decrease is obtained using a climate optimization of the final hybrid-electric aircraft fleet (case D.). Emissions can be reduced with 38% with respect to the kerosene fleet.

## Acknowledgments

## References

[1] Felder, J. L., "NASA Electric Propulsion System Studies," *5th EnergyTech 2015*, Cleveland, OH, United States, 2015.

[2] Borer, N. K., Patterson, M. D., Viken, J. K., Moore, M. D., Clarke, S., Redifer, M. E., Christie, R. J., Stoll, A. M., Dubois, A., Bevirt, J. B., Gibson, A. R., Foster, T. J., and Osterkamp, P. G., "Design and Performance of the NASA SCEPTOR Distributed Electric Propulsion Flight Demonstrator," *16th AIAA Aviation Technology, Integration, and Operations Conference, Washington, DC, USA*, American Institute of Aeronautics and Astronautics, American Institute of Aeronautics and Astronautics, 2016. https://doi.org/10.2514/6.2016-3920.

[3] Antcliff, K. R., and Capristan, F. M., "Conceptual Design of the Parallel Electric-Gas Architecture with Synergistic Utilization Scheme (PEGASUS) Concept," *18th AIAA/ISSMO Multidisciplinary Analysis and Optimization Conference*, American Institute of Aeronautics and Astronautics, 2017. https://doi.org/10.2514/6.2017-4001.

[4] Rothhaar, P. M., Murphy, P. C., Bacon, B. J., Gregory, I. M., Grauer, J. A., Busan, R. C., and Croom, M. A., "NASA langley distributed propulsion VTOL tilt-wing aircraft testing, modeling, simulation, control, and flight test development," *Proceedings of the 14th AIAA Aviation Technology, Integration, and Operations Conference, Atlanta, GA, USA*, American Institute of Aeronautics and Astronautics, American Institute of Aeronautics and Astronautics, 2014. https://doi.org/10.2514/6.2014-2999.

[5] Schiltgen, B. T., and Freeman, J., "Aeropropulsive interaction and thermal system integration within the ECO-150: a turboelectric distributed propulsion airliner with conventional electric machines," *16th AIAA Aviation Technology, Integration, and Operations Conference, Washington, DC, USA*, American Institute of Aeronautics and Astronautics, 2016. https://doi.org/10.2514/6.2016-4064.

[6] Hermetz, J., Ridel, M., and Döll, C., "Distributed electric propulsion for small business aircraft: A concept-plane for key-technologies investigations," *Proceedings of the 30th Congress of the International Council of the Aeronautical Sciences, Daejeon, South Korea*, International Council of the Aeronautical Sciences, 2016.

[7] Stoll, A. M., and Mikić, G. V., "Design Studies of Thin-Haul Commuter Aircraft with Distributed Electric Propulsion," *16th AIAA Aviation Technology, Integration and Operations Conference, Washington, DC, USA*, American Institute of Aeronautics and Astronautics, American Institute of Aeronautics and Astronautics, 2016. https://doi.org/10.2514/6.2016-3765.

[8] Jansen, R. H., Bowman, C., Jankovsky, A., Dyson, R., and Felder, J., "Overview of NASA Electrified Aircraft Propulsion Research for Large Subsonic Transports," *53rd AIAA/SAE/ASEE Joint Propulsion Conference, Atlanta, GA, USA*, American Institute of Aeronautics and Astronautics, American Institute of Aeronautics and Astronautics, 2017. https://doi.org/10.2514/6.2017-4701.

[9] Steiner, H. J., Seitz, A., Wieczorek, K., Plötner, K., Iskiveren, A. T., and Hornung, M., "Multi-disciplinary design and feasibility study of distributed propulsion systems," *Proceedings of the 28th ICAS Congress, Brisbane, Australia*, International Council of the Aeronautical Sciences, 2012.

[10] Voskuijl, M., Van Bogaert, J., and Rao, A., "Analysis and Design of Hybrid Electric Regional Turboprop Aircraft," *CEAS Aeronautical Journal*, Vol. 9, No. 1, 2018, pp. 15–25. https://doi.org/10.1007/s13272-017-0272-1.

[11] de Vries, R., Hoogreef, M. F. M., and Vos, R., "Preliminary Sizing of a Hybrid-Electric Passenger Aircraft Featuring Over-the-Wing Distributed-Propulsion," *AIAA SciTech 2019 Forum*, American Institute of Aeronautics and Astronautics, 2019. https://doi.org/10.2514/6.2019-1811.

[12] Hoogreef, M. F. M., Vos, R., de Vries, R., and Veldhuis, L. L. M., "Conceptual Assessment of Hybrid Electric Aircraft with Distributed Propulsion and Boosted Turbofans," *AIAA SciTech 2019 Forum*, American Institute of Aeronautics and Astronautics, 2019. https://doi.org/10.2514/6.2019-1807.

[13] Zamboni, J., Vos, R., Emeneth, M., and Schneegans, A., "A method for the conceptual design of hybrid electric aircraft," *AIAA SciTech 2019 Forum*, American Institute of Aeronautics and Astronautics, 2019. https://doi.org/10.2514/6.2019-1587.

[14] de Vries, R., Brown, M., and Vos, R., "Preliminary Sizing Method for Hybrid-Electric Distributed-Propulsion Aircraft," *Journal of Aircraft*, Vol. 56, No. 6, 2019, pp. 1–17. https://doi.org/10.2514/1.c035388.

[15] Finger, D. F., Bil, C., and Braun, C., "Initial sizing methodology for hybrid-electric general aviation aircraft," *Journal of Aircraft*, Vol. 57, No. 2, 2020, pp. 245–255. https://doi.org/10.2514/1.C035428.

[16] Belobaba, P., Odoni, A., and Barnhart, C., *The Global Airline Industry*, 2nd ed., John Wiley & Sons, 2009.

[17] Schick, G., and Stroup, J., "Experience with a multi-year fleet planning model," *Omega*, Vol. 9, No. 4, 1981, pp. 389–396. https://doi.org/10.1016/0305-0483(81)90083-9.

[18] Oum, T. H., Zhang, A., and Zhang, Y., "Optimal demand for operating lease of aircraft," *Transportation Research Part B: Methodological*, Vol. 34, No. 1, 2000, pp. 17–29. https://doi.org/10.1016/S0191-2615(99)00010-7.

[19] Listes, O., and Dekker, R., "A Scenario Aggregation—Based Approach for Determining a Robust Airline Fleet Composition for Dynamic Capacity Allocation," *Transportation Science*, Vol. 39, No. 3, 2005, pp. 367–382. URL http://www.jstor.org/stable/25769257.

[20] Khoo, H. L., and Teoh, L. E., "An optimal aircraft fleet management decision model under uncertainty," *Journal of Advanced Transportation*, Vol. 48, No. 7, 2014, pp. 798–820. https://doi.org/10.1002/atr.1228.

[21] Repko, M. G., and Santos, B. F., "Scenario tree airline fleet planning for demand uncertainty," *Journal of Air Transport Management*, Vol. 65, 2017, pp. 198–208. https://doi.org/10.1016/j.jairtraman.2017.06.010.

[22] Sa, C. A., Santos, B. F., and Clarke, J.-P. B., "Portfolio-based airline fleet planning under stochastic demand," *Omega*, Vol. 97, 2020, p. 102101. https://doi.org/10.1016/j.omega.2019.08.008, URL https://www.sciencedirect.com/science/article/pii/S0305048318304833.

[23] de Koning, M., "Fleet planning under Demand Uncertainty: a Reinforcement Learning Approach," Msc thesis, 2021. URL http://resolver.tudelft.nl/uuid:67125be4-e9d3-46c6-9983-300d71b3511f.

[24] Geursen, I. L., "Fleet Planning Under Demand and Fuel Price Uncertainty," Msc thesis, 2021. URL http://resolver.tudelft.nl/uuid:1eed4184-5c4a-4e88-b54d-8c9751f79ebf.

[25] Khoo, H. L., and Teoh, L. E., "A bi-objective dynamic programming approach for airline green fleet planning," *Transportation Research Part D: Transport and Environment*, Vol. 33, 2014, pp. 166–185. https://doi.org/10.1016/j.trd.2014.06.003, URL https://www.sciencedirect.com/science/article/pii/S1361920914000686.

[26] Jaillet, P., Song, G., and Yu, G., "Airline network design and hub location problems," *Location Science*, Vol. 4, No. 3, 1996, pp. 195–212. https://doi.org/10.1016/S0966-8349(96)00016-2, URL https://www.sciencedirect.com/science/article/pii/S0966834996000162, hub Location.

[27] Evans, A., Schafer, A., and Dray, L., *Modelling Airline Network Routing and Scheduling under Airport Capacity Constraints*, 2008. https://doi.org/10.2514/6.2008-8855.

[28] Wang, D. D., Klabjan, D., and Shebalov, S., "Attractiveness-Based Airline Network Models with Embedded Spill and Recapture," *Journal of Airline and Airport Management*, Vol. 4, No. 1, 2014, pp. 1–25. https://doi.org/10.3926/jairm.20, URL https://www.jairm.org/index.php/jairm/article/view/20.

[29] Crossley, W., Mane, M., and Nusawardhana, A., "Variable resource allocation using multidisciplinary optimization: Initial investigations for system of systems," *10th AIAA/ISSMO multidisciplinary analysis and optimization conference*, 2004, p. 4605. https://doi.org/10.2514/6.2004-4605.

[30] Crossley, W., and Mane, M., *System of Systems Inspired Aircraft Sizing Applied to Commercial Aircraft / Airline Problems*, 2005. https://doi.org/10.2514/6.2005-7426.

[31] Mane, M., Crossley, W. A., and Nusawardhana, "System-of-systems inspired aircraft sizing and airline resource allocation via decomposition," *Journal of aircraft*, Vol. 44, No. 4, 2007, pp. 1222–1235. https://doi.org/10.2514/1.26333.

[32] Mane, M., and Crossley, W., "Concurrent Aircraft Design and Resource Allocation Under Uncertainty for On-Demand Air Transportation," *The 26th Congress of ICAS and 8th AIAA ATIO*, 2008, p. 8903.

[33] Mane, M., and Crossley, W., "Concurrent aircraft design and trip assignment under uncertainty: Fractional operations," *9th AIAA Aviation Technology, Integration, and Operations Conference (ATIO) and Aircraft Noise and Emissions Reduction Symposium (ANERS)*, 2009, p. 7007. https://doi.org/10.2514/6.2009-7007.

[34] Mane, M., and Crossley, W. A., "Allocation and design of aircraft for on-demand air transportation with uncertain operations," *Journal of aircraft*, Vol. 49, No. 1, 2012, pp. 141–150. https://doi.org/10.2514/1.C031452.

[35] Taylor, C., and de Weck, O., *Integrated Transportation Network Design Optimization*, 2006. https://doi.org/10.2514/6.2006-1912.

[36] Taylor, C., and De Weck, O. L., "Coupled vehicle design and network flow optimization for air transportation systems," *Journal of Aircraft*, Vol. 44, No. 5, 2007, pp. 1479–1486.

[37] Nusawardhana, N., and Crossley, W., *Concurrent Aircraft Design and Variable Resource Allocation in Large Scale Fleet Networks*, 2009. https://doi.org/10.2514/6.2009-6977.

[38] Davendralingam, N., and Crossley, W., *Concurrent Aircraft Design and Airline Network Design Incorporating Passenger Demand Models*, 2009. https://doi.org/10.2514/6.2009-6971.

[39] Hwang, J., Roy, S., Kao, J., Martins, J. R. R. A., and Crossley, W. A., *Simultaneous aircraft allocation and mission optimization using a modular adjoint approach*, American Institute of Aeronautics and Astronautics, 2015. https://doi.org/10.2514/6.2015-0900.

[40] Hwang, J. T., and Martins, J. R., "Parallel allocation-mission optimization of a 128-route network," *16th AIAA/ISSMO Multidisciplinary Analysis and Optimization Conference*, American Institute of Aeronautics and Astronautics, 2015, p. 2321. https://doi.org/10.2514/6.2015-2321.

[41] Hwang, J. T., and Martins, J. R. R. A., "Allocation-mission-design optimization of next-generation aircraft using a parallel computational framework," *57th AIAA/ASCE/AHS/ASC Structures, Structural Dynamics, and Materials Conference*, American Institute of Aeronautics and Astronautics, 2016. https://doi.org/10.2514/6.2016-1662.

[42] Roy, S., and Crossley, W. A., "An EGO-like optimization framework for simultaneous aircraft design and airline allocation," *57th AIAA/ASCE/AHS/ASC Structures, Structural Dynamics, and Materials Conference*, American Institute of Aeronautics and Astronautics, 2016, p. 1659. https://doi.org/10.2514/6.2016-1659.

[43] Roy, S., Moore, K., Hwang, J. T., Gray, J. S., Crossley, W. A., and Martins, J. R. R. A., *A Mixed Integer Efficient Global Optimization Algorithm for the Simultaneous Aircraft Allocation-Mission-Design Problem*, 2017. https://doi.org/10.2514/6.2017-1305.

[44] Alexandre, J., Fregnani, T., De Mattos, B. S., and Hernandes, J. A., "An innovative approach for integrated airline network and aircraft family optimization," *Chinese Journal of Aeronautics*, Vol. 33, No. 2, 2020, pp. 634–663. https://doi.org/10.1016/j.cja.2019.10.004, URL https://www.sciencedirect.com/science/article/pii/S1000936119304042.

[45] Husemann, M., Schäfer, K., and Stumpf, E., "Flexibility within flight operations as an evaluation criterion for preliminary aircraft design," Vol. 71, 2018, pp. 201–214. https://doi.org/10.1016/j.jairtraman.2018.04.007, URL https://www.sciencedirect.com/science/article/pii/S0969699718301431.

[46] Lehner, S., Zill, T., and Gollnick, V., "Using Aircraft Requirements as Variables: An Integrated Optimization Approach for Air Transportation Systems," No. 0 in Aviation Technology, Integration, and Operations (ATIO) Conferences, American Institute of Aeronautics and Astronautics, 2012. https://doi.org/10.2514/6.2012-5680, URL https://doi.org/10.2514/6.2012-5680.

[47] Marwaha, G., and Kokkolaras, M., "System-of-systems approach to air transportation design using nested optimization and direct search," Vol. 51, No. 4, 2015, pp. 885–901. https://doi.org/10.1007/s00158-014-1180-1, URL https://doi.org/10.1007/s00158-014-1180-1.

[48] Jansen, P., and Perez, R., "Coupled optimization of aircraft family design and fleet assignment for minimum cost and fuel burn," *12th AIAA Aviation Technology, Integration, and Operations (ATIO) Conference and 14th AIAA/ISSMO Multidisciplinary Analysis and Optimization Conference*, American Institute of Aeronautics and Astronautics, 2012, p. 5495. https://doi.org/10.2514/6.2012-5495.

[49] Jansen, P. W., and Perez, R. E., "Coupled optimization of aircraft design and fleet allocation with uncertain passenger demand," *2013 Aviation Technology, Integration, and Operations Conference*, American Institute of Aeronautics and Astronautics, 2013, p. 4392. https://doi.org/10.2514/6.2013-4392.

[50] Perez, R. E., and Jansen, P. W., "Effect of Passenger Preferences on the Integrated Design and Optimization of Aircraft Families and Air Transport Network," AIAA AVIATION Forum, American Institute of Aeronautics and Astronautics, 2017. https://doi.org/10.2514/6.2017-4249, URL https://doi.org/10.2514/6.2017-4249.

[51] Jansen, P. W., and Perez, R. E., "Robust Coupled Optimization of Aircraft Design and Fleet Allocation for Multiple Markets," *AIAA/3AF Aircraft Noise and Emissions Reduction Symposium*, American Institute of Aeronautics and Astronautics, 2014, p. 2735. https://doi.org/10.2514/6.2014-2735.

[52] Jansen, P. W., and Perez, R. E., "Coupled Optimization of Aircraft Families and Fleet Allocation for Multiple Markets," *Journal of Aircraft*, Vol. 53, No. 5, 2016, pp. 1485–1504. https://doi.org/10.2514/1.C033646.

[53] Reid, S. J., Perez, R. E., Jansen, P. W., and Bil, C., "Influence of Carbon Pricing on Regional Aircraft and Route Network Design," AIAA SciTech Forum, American Institute of Aeronautics and Astronautics, 2021. https://doi.org/10.2514/6.2021-0463, URL https://doi.org/10.2514/6.2021-0463.

[54] Schwartz, E., and Kroo, I., "Aircraft Design: Trading Cost and Climate Impact," American Institute of Aeronautics and Astronautics, 2009. https://doi.org/10.2514/6.2009-1261, URL https://doi.org/10.2514/6.2009-1261.

[55] Bower, G., and Kroo, I., "Multi-objective aircraft optimization for minimum cost and emissions over specific route networks," *The 26th Congress of ICAS and 8th AIAA ATIO*, 2008, p. 8905. https://doi.org/10.2514/6.2008-8905.

[56] Govindaraju, P., Davendralingam, N., and Crossley, W. A., "A Concurrent Aircraft Design and Fleet Assignment Approach to Mitigate Environmental Impact through Fuel Burn Reduction under Operational Uncertainty," *Journal of Aerospace Operations*, Vol. 4, No. 4, 2017, pp. 163–184. https://doi.org/10.3233/AOP-170061.

[57] Weit, C. J., Justin, C. Y., and Mavris, D. N., "Network-Optimized Design of a Notional Hybrid Electric Airplane for Thin-Haul Operations," *AIAA Aviation 2019 Forum*, 2019, p. 3002. https://doi.org/10.2514/6.2019-3002.

[58] Roskam, J., *Airplane Design*, DAR corporation, DARcorporation, Lawrence, KS, 1985.

[59] Proesmans, P., and Vos, R., "Airplane Design Optimization for Minimal Global Warming Impact," *Journal of Aircraft*, Vol. 59, No. 5, 2022, pp. 1363–1381. https://doi.org/10.2514/1.C036529.

[60] National Academies of Sciences, E., and Medicine, *Commercial Aircraft Propulsion and Energy Systems Research: Reducing Global Carbon Emissions*, The National Academies Press, Washington, DC, 2016.

[61] Rheaume, J. M., and Lents, C., "Energy Storage for Commercial Hybrid Electric Aircraft," *SAE 2016 Aerospace Systems and Technology Conference*, SAE International, 2016. https://doi.org/10.4271/2016-01-2014.

[62] Stückl, S., van Toor, J., and Lobentanzer, H., "VOLTAIR-the all electric propulsion concept platform–a vision for atmospheric friendly flight," *28th International Congress of the Aeronautical Sciences (ICAS)*, International Council of the Aeronautical Sciences, 2012.

[63] Fefermann, Y., Maury, C., Level, C., Zarati, K., Salanne, J.-P., Pornet, C., Thoraval, B., and Isikveren, A., "Hybrid-Electric Motive Power Systems for Commuter Transport Applications," *Proceedings of the 30th Congress of the International Council of the Aeronautical Sciences, Daejeon, South Korea*, International Council of the Aeronautical Sciences, 2016.

[64] Jones, S. M., Haller, W., and Tong, M., "An N+3 Technology Level Reference Propulsion System," Tech. Rep. 2017-219501, NASA, 2017.

[65] de Vries, R., "Hybrid-Electric Aircraft with Over-the-Wing Distributed Propulsion: Aerodynamic Performance and Conceptual Design," Ph.D. thesis, Delft University of Technology, 2022.

[66] de Vries, R., Brown, M. T., and Vos, R., "A Preliminary Sizing Method for Hybrid-Electric Aircraft Including Aero-Propulsive Interaction Effects," *AIAA AVIATION 2018 Forum*, American Institute of Aeronautics and Astronautics, 2018. https://doi.org/10.2514/6.2018-4228.

[67] Torenbeek, E., *Synthesis of Subsonic Airplane Design*, Delft Univ. Press, Delft, The Netherlands, 1982.

[68] Thijssen, R., "Propeller Aircraft Design Optimization for Reduced Climate Impact," Master's thesis, Delft University of Technology, 2022.

[69] Obert, E., "Drag polars of nineteen jet transport aircraft at Mach numbers M= 0.40-0.60 (unpublished)," Tech. rep., 2013.

[70] Teeuwen, Y., "Propeller Design for Conceptual Turboprop Aircraft," Master's thesis, Delft University of Technology, 2017.

[71] de Vries, R., Hoogreef, M. F. M., and Vos, R., "Range Equation for Hybrid-Electric Aircraft with Constant Power Split," *Journal of Aircraft*, Vol. 57, No. 3, 2020, pp. 552–557. https://doi.org/10.2514/1.C035734.

[72] Gurobi Optimization, LLC, "Gurobi Optimizer Reference Manual," , 2023. URL https://www.gurobi.com.

[73] Scholz, A. E., Michelmann, J., and Hornung, M., "Design, Operational and Environmental Assessment of a Hybrid-Electric Aircraft," *AIAA Scitech 2021 Forum*, 2021, p. 0259.

[74] Raymer, D., *Aircraft design: a conceptual approach*, American Institute of Aeronautics and Astronautics, Inc., 2012.

[75] Elmendorp, R. J. M., Vos, R., and La Rocca, G., "A Conceptual Design and Analysis Method for Conventional and Unconventional Airplanes," *ICAS 2014: Proceedings of the 29th Congress of the International Council of the Aeronautical Sciences, St. Petersburg, Russia, 7-12 September 2014*, International Council of Aeronautical Sciences, 2014. URL https://repository.tudelft.nl/islandora/object/uuid%3A1dc55ce5-18c3-4986-b668-f70d9b24aac0.

[76] Hoogreef, M. F. M., de Vries, R., Sinnige, T., and Vos, R., "Synthesis of Aero-Propulsive Interaction Studies Applied to Conceptual Hybrid-Electric Aircraft Design," *AIAA SciTech 2020 Forum*, American Institute of Aeronautics and Astronautics, 2020. https://doi.org/10.2514/6.2020-0503, URL https://repository.tudelft.nl/islandora/object/uuid%3A2cf180a6-9e0f-417a-af41-45585ea8281d.

[77] La Rocca, G., Langen, T., , and Brouwers, Y., "The design and engineering engine. Towards a modular system for collaborative aircraft design," *28th International Congress of the Aeronautical Sciences (ICAS)*, International Council of the Aeronautical Sciences, 2012.

[78] Finger, D. F., de Vries, R., Braun, C., Vos, R., and Bil, C., "A Comparison of Hybrid-Electric Aircraft Sizing Methods," *AIAA SciTech 2020 Forum*, American Institute of Aeronautics and Astronautics, 2020. https://doi.org/10.2514/6.2020-1006.

[79] Finger, D. F., de Vries, R., Vos, R., Braun, C., and Bil, C., "Cross-Validation of Hybrid-Electric Aircraft Sizing Methods," *Journal of Aircraft*, 2022, pp. 1–19. https://doi.org/10.2514/1.C035907.

# Appendices

The following tables and figures provide, requirements for initial hybrid fleet and an overview of the designed aircraft and the redesign process for case study 2.

**Table 15    TLAR for HE Q400 and HE Q200**

| Parameter | Unit | HE Q400 | HE Q200 |
|---|---|---|---|
| **Capacity** | | | |
| Passengers | – | 80 | 37 |
| Mass per passenger | $kg$ * | 110 | 110 |
| **Design Mission** | | | |
| Cruise range | $km$ | 900 | 1000 |
| Cruise altitude | $m$ | 7010.4 | 7600 |
| Cruise velocity | $m/s$ | 182 | 150 |
| Diversion range | $km$* | 185.2 | 185.2 |
| Diversion altitude | $m$* | 1524 | 1524 |
| Diversion velocity | $m/s$ | 182 | 150 |
| Loiter time | $s$* | 2700 | 2700 |
| Loiter altitude | $m$* | 457.2 | 457.2 |
| **Mission hybrid power control parameters** | | | |
| Supplied power split (all phases) | –* | 0.0485 | 0.0485 |
| Shaft power split (all phases) | –* | 0 | 0 |
| Turbine Throttle (all phases) | –* | 1 | 1 |
| **Aircraft configuration/geometry** | | | |
| Undercarriage configuration* | | In nacelle | In nacelle |
| Wing configuration* | | High wing | High wing |
| Horizontal tail configuration* | | T-tail | T-tail |
| Aspect ratio* | – | 12.5 | 12.5 |
| **Loading requirements** | | | |
| Cruise speed | $m/s$ | 182 | 150 |
| Cruise altitude | $m$ | 7010.4 | 7600 |
| Stall speed | $m/s$ | 47 | 41 |
| Take-off distance | $m$ | 1300 | 1000 |
| Climb gradient OEI | %* | 2.4 | 2.4 |

---

*Parameter identical for all hybrid-electric aircraft.

**Table 16  Hybrid-electric HE Q400 and HE Q200 design results**

| Aircraft name: HE Q400 | Seats [-] | Cruise Range [km] | Total Range [km] | Speed [km/h] | Altitude [m] | Runway length [m] | Φ cruise [-] | max_energy [kWh] | max_fuel [kg] | energy_stop [kWh] | energy_km [kWh/km] | fuel_stop [kg] | fuel_km [kg/km] |
|---|---|---|---|---|---|---|---|---|---|---|---|---|---|
| On_design-80-1109-1300 | 80 | 900 | 1109 | 655.2 | 7010.4 | 1300 | 0.0485 | 1361 | 1869 | 527 | 0.93 | 724 | 1.27 |
| Off_design-70-1483-1258 | 70 | 1274 | 1483 | 655.2 | 7010.4 | 1258 | 0.0485 | 1361 | 2359 | 527 | 0.65 | 708 | 1.30 |
| Off_design-60-1852-1216 | 60 | 1643 | 1852 | 655.2 | 7010.4 | 1216 | 0.0485 | 1361 | 2848 | 527 | 0.51 | 691 | 1.31 |
| Off_design-50-2220-1175 | 50 | 2011 | 2220 | 655.2 | 7010.4 | 1175 | 0.0485 | 1361 | 3337 | 527 | 0.41 | 674 | 1.32 |
| Off_design-40-2589-1134 | 40 | 2380 | 2589 | 655.2 | 7010.4 | 1134 | 0.0485 | 1361 | 3827 | 527 | 0.35 | 658 | 1.33 |
| Off_design-30-2958-1094 | 30 | 2749 | 2958 | 655.2 | 7010.4 | 1094 | 0.0485 | 1361 | 4317 | 527 | 0.30 | 641 | 1.34 |
| Off_design-20-3327-1054 | 20 | 3118 | 3327 | 655.2 | 7010.4 | 1054 | 0.0485 | 1361 | 4807 | 527 | 0.27 | 624 | 1.34 |
| Off_design-10-3695-1023 | 10 | 3486 | 3695 | 655.2 | 7010.4 | 1023 | 0.0485 | 1361 | 5295 | 527 | 0.24 | 608 | 1.34 |
| Off_design-70-1109-1224 | 70 | 900 | 1109 | 655.2 | 7010.4 | 1224 | 0.0485 | 1361 | 1830 | 527 | 0.93 | 704 | 1.25 |
| Off_design-60-1109-1150 | 60 | 900 | 1109 | 655.2 | 7010.4 | 1150 | 0.0485 | 1361 | 1792 | 527 | 0.93 | 682 | 1.23 |
| Off_design-50-1109-1075 | 50 | 900 | 1109 | 655.2 | 7010.4 | 1075 | 0.0485 | 1361 | 1753 | 527 | 0.93 | 660 | 1.21 |
| Off_design-40-1109-1018 | 40 | 900 | 1109 | 655.2 | 7010.4 | 1018 | 0.0485 | 1361 | 1715 | 527 | 0.93 | 638 | 1.20 |
| Off_design-30-1109-983 | 30 | 900 | 1109 | 655.2 | 7010.4 | 983 | 0.0485 | 1361 | 1676 | 527 | 0.93 | 616 | 1.18 |
| Off_design-20-1109-949 | 20 | 900 | 1109 | 655.2 | 7010.4 | 949 | 0.0485 | 1361 | 1639 | 527 | 0.93 | 595 | 1.16 |
| Off_design-10-1109-914 | 10 | 900 | 1109 | 655.2 | 7010.4 | 914 | 0.0485 | 1361 | 1600 | 527 | 0.93 | 573 | 1.14 |

| Aircraft name: HE Q200 | Seats [-] | Cruise Range [km] | Total Range [km] | Speed [km/h] | Altitude [m] | Runway length [m] | Φ cruise [-] | max_energy [kWh] | max_fuel [kg] | energy_stop [kWh] | energy_km [kWh/km] | fuel_stop [kg] | fuel_km [kg/km] |
|---|---|---|---|---|---|---|---|---|---|---|---|---|---|
| On_design-37-1226-1000 | 37 | 1000 | 1226 | 540 | 7600 | 1000 | 0.0485 | 692 | 950 | 272 | 0.42 | 374 | 0.58 |
| Off_design-27-2053-938 | 27 | 1827 | 2053 | 540 | 7600 | 938 | 0.0485 | 692 | 1439 | 272 | 0.23 | 357 | 0.59 |
| Off_design-17-2884-875 | 17 | 2658 | 2884 | 540 | 7600 | 875 | 0.0485 | 692 | 1929 | 272 | 0.16 | 340 | 0.60 |
| Off_design-7-3714-814 | 7 | 3488 | 3714 | 540 | 7600 | 814 | 0.0485 | 692 | 2418 | 272 | 0.12 | 323 | 0.60 |
| Off_design-27-1226-887 | 27 | 1000 | 1226 | 540 | 7600 | 887 | 0.0485 | 692 | 908 | 272 | 0.42 | 353 | 0.56 |
| Off_design-17-1226-784 | 17 | 1000 | 1226 | 540 | 7600 | 784 | 0.0485 | 692 | 865 | 272 | 0.42 | 330 | 0.54 |
| Off_design-7-1226-731 | 7 | 1000 | 1226 | 540 | 7600 | 731 | 0.0485 | 692 | 824 | 272 | 0.42 | 308 | 0.52 |

**Table 17    Final Hybrid-electric aircraft fleet**

| Aircraft name | Seats [-] | Cruise Range [km] | Total Range [km] | Speed [km/h] | Altitude [m] | Runway length [m] | Φ cruise [-] | max_ energy [kWh] | max_ fuel [kg] | energy_ stop [kWh] | energy_ km [kWh/km] | fuel_ stop [kg] | fuel_ km [kg/km] |
|---|---|---|---|---|---|---|---|---|---|---|---|---|---|
| On_design-80-1109-1300 | 80 | 900 | 1109 | 655.2 | 7010.4 | 1300 | 0.0485 | 1361 | 1869 | 527 | 0.93 | 724 | 1.27 |
| On_design-70-809-1250 | 70 | 600 | 809 | 655.2 | 7010.4 | 1250 | 0.0485 | 932 | 1281 | 443 | 0.82 | 608 | 1.12 |
| On_design-70-309-1550 | 70 | 100 | 309 | 655.2 | 7010.4 | 1550 | 0.0485 | 451 | 619 | 380 | 0.71 | 523 | 0.97 |
| On_design-7-1126-750 | 7 | 900 | 1126 | 540 | 7600 | 750 | 0.0485 | 341 | 468 | 124 | 0.24 | 170 | 0.33 |
| On_design-17-826-750 | 17 | 600 | 826 | 540 | 7600 | 750 | 0.0485 | 370 | 508 | 177 | 0.32 | 244 | 0.44 |
| On_design-37-1126-1250 | 37 | 900 | 1126 | 540 | 7600 | 1250 | 0.0485 | 592 | 813 | 248 | 0.38 | 341 | 0.52 |

**Table 18    Climate optimized Final Hybrid-electric aircraft fleet**

| Aircraft name | Seats [-] | Cruise Range [km] | Total Range [km] | Speed [km/h] | Altitude [m] | Runway length [m] | Φ cruise [-] | max_ energy [kWh] | max_ fuel [kg] | energy_ stop [kWh] | energy_ km [kWh/km] | fuel_ stop [kg] | fuel_ km [kg/km] |
|---|---|---|---|---|---|---|---|---|---|---|---|---|---|
| On_design-80-1109-1300 | 80 | 958 | 1109 | 501 | 5066 | 1300 | 0.0476 | 998 | 1388 | 338 | 0.69 | 464 | 0.97 |
| On_design-70-809-1250 | 70 | 663 | 809 | 487 | 4907 | 1250 | 0.0636 | 806 | 928 | 282 | 0.79 | 388 | 0.82 |
| On_design-70-309-1550 | 70 | 163 | 309 | 487 | 4907 | 1550 | 0.0810 | 397 | 461 | 250 | 0.90 | 344 | 0.72 |
| On_design-7-1126-750 | 7 | 952 | 1126 | 432 | 5856 | 750 | 0.0570 | 316 | 386 | 90 | 0.24 | 123 | 0.28 |
| On_design-17-826-750 | 17 | 668 | 826 | 432 | 5320 | 750 | 0.0575 | 341 | 418 | 119 | 0.33 | 163 | 0.38 |
| On_design-37-1126-1250 | 37 | 968 | 1126 | 432 | 5320 | 1250 | 0.0619 | 630 | 723 | 174 | 0.47 | 239 | 0.50 |
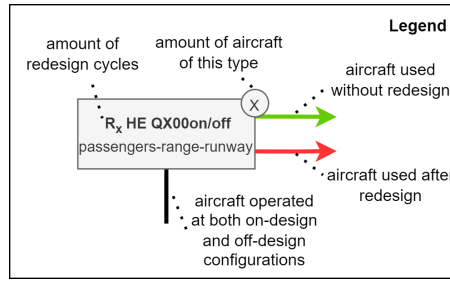
(a) Legend
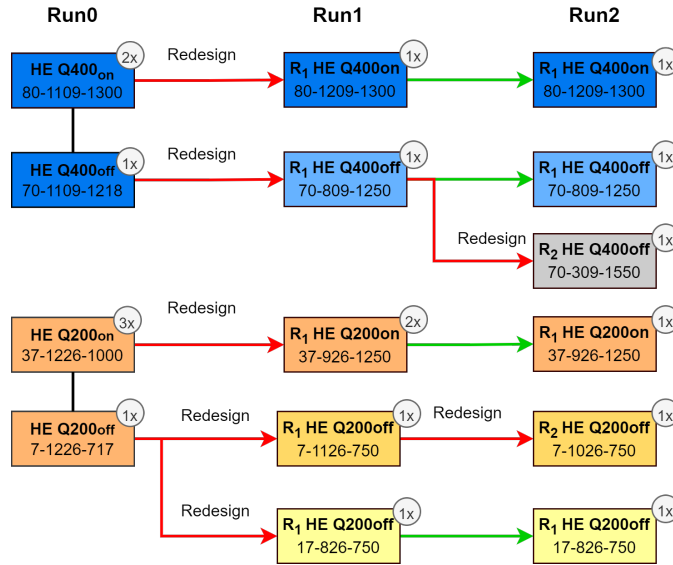


(b) Technology sensitivity study - Battery specific energy $700 Wh/kg$
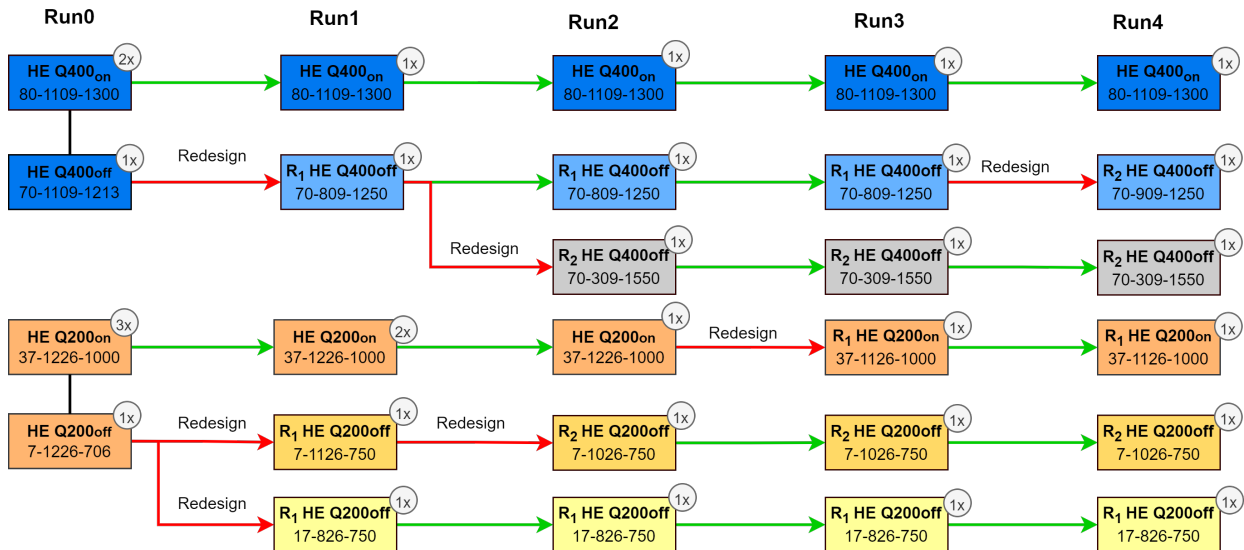


(c) Technology sensitivity study - Battery specific energy $1000 Wh/kg$

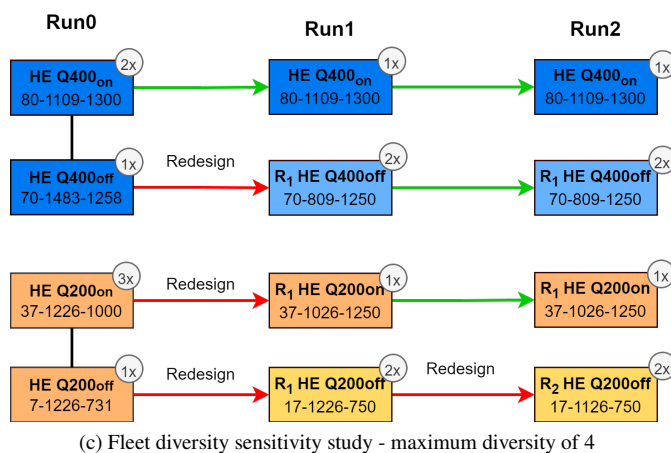**Fig. 22   Schematic of aircraft redesign cycles for battery technology sensitivities.**

(a) Fleet diversity sensitivity study - maximum diversity of 2



(b) Fleet diversity sensitivity study - maximum diversity of 3



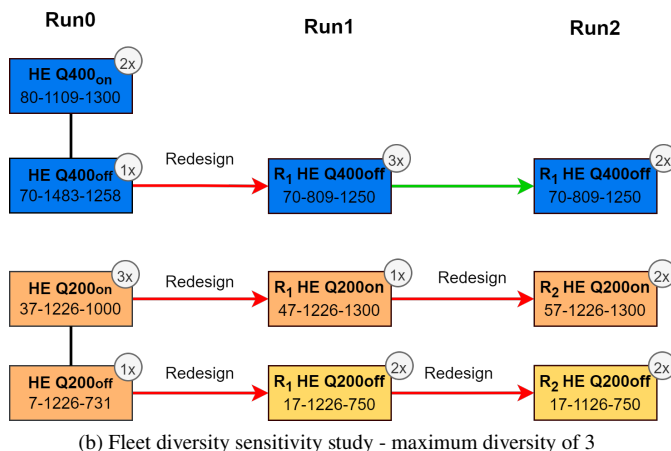(c) Fleet diversity sensitivity study - maximum diversity of 4
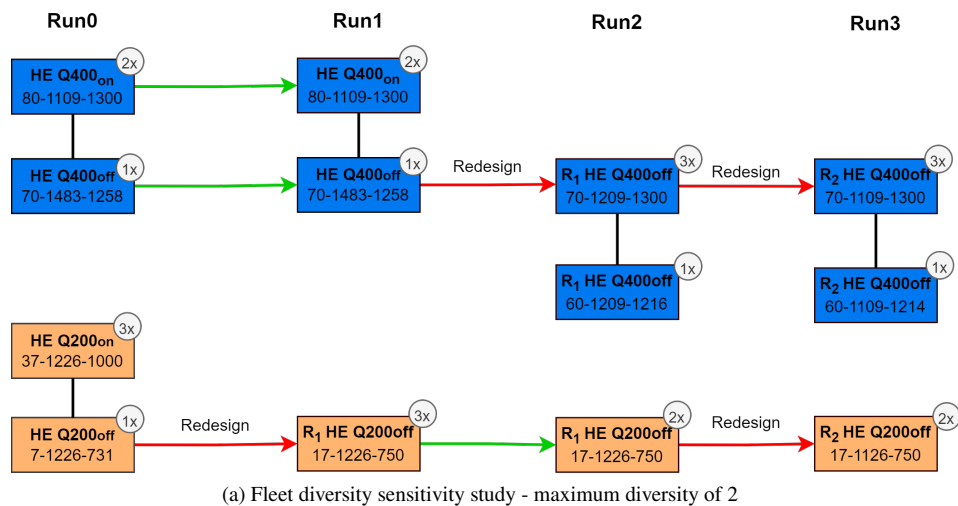
**Fig. 23    Schematic of aircraft redesign cycles for fleet diversity sensitivities.**